Metabolic and genomic adaptations of *Salmonella* Typhimurium grown on itaconate

Jacob Pierscianowski[1], Suzana Diaconescu-Grabari[1], Farhan R. Chowdhury[2], Andréanne Lupien[3,4,5,6], Brandon L. Findlay[2,7], Karine Auclair[1]*

[1]*Department of Chemistry, McGill University, Montreal, Canada*

[2]*Department of Chemistry and Biochemistry, Concordia University, Montreal, Canada*

[3]*Department of Microbiology and Immunology, McGill University, Montreal, Canada*

[4]*McGill International TB Centre, Montreal, QC, Canada*

[5]*The Infectious Diseases and Immunity in Global Health Program, The Research Institute of the McGill University Health Centre, Montreal, QC, Canada*

[6]*Department of Medicine, McGill University, Montreal, QC, Canada*

[7]*Department of Biology, Concordia University, Montreal, Canada*

* Corresponding author

Email: k.auclair@mcgill.ca (KA)

23 Abstract

24 *Salmonella enterica* ser. Typhimurium (STm) is an enteric pathogen that causes almost 100 million
25 cases of salmonellosis a year. A hallmark of STm is their ability to survive and replicate in the
26 macrophages that phagocytose them. Inside the *Salmonella*-containing vesicles (SCV) STm is exposed
27 to nutrient limitation and antimicrobial molecules, including itaconate, a dicarboxylate produced at
28 millimolar concentrations by activated macrophages. STm has an itaconate degradation pathway that
29 allows it to detoxify itaconate and convert it into pyruvate and acetyl-CoA. In the SCV, STm undergoes
30 extensive metabolic reprogramming in response to the nutrient limitation and high stress environment,
31 and strict catabolite control is employed at various stages of infection, depending on carbon source
32 availability. The extent to which itaconate is used as a carbon source by STm is not currently well
33 understood. Here, we explore the ability of STm to grow in media containing itaconate as the sole
34 carbon source, identify the genes of the itaconate response operon necessary for itaconate degradation,
35 and confirm their importance during infection of macrophages. Growth on itaconate was substantially
36 slower than in carbon-rich or acetate media, with multiple subcultures allowing for increased growth
37 rates. Genomic analysis suggests that mutations in the RpoS-stress response and increased expression of
38 the DctA transporter improve growth on itaconate. Using metabolomics, it was revealed that growth on
39 itaconate resulted in substantially reduced levels of gluconeogenesis compared to growth on acetate and
40 increased glutathione disulfide levels, indicating a high level of oxidative stress. Overall, our results
41 point towards the STm itaconate degradation pathway having a more important role in detoxifying
42 itaconate, rather than using it as a carbon source inside the macrophage. Additionally, this study
43 establishes media conditions that would enable the high throughput discovery of potential inhibitors of
44 itaconate degradation.

46 Author Summary

47 *Salmonella enterica* serovar Typhimurium (STm) is commonly linked to foodborne illness, but it is also
48 known to cause severe systemic infections. Due to this and the prevalence of antibiotic resistance, the
49 World Health Organization has identified STm as a high-priority pathogen. STm resilience during
50 infection is due in part to its ability to thrive in a wide range of environments, including the hostile
51 conditions inside macrophages—immune cells designed to kill invading bacteria. STm survives in part
52 by degrading itaconate, an antimicrobial molecule produced by macrophages. While the importance of
53 this degradation pathway for STm intracellular survival is known, the broader benefits of itaconate
54 metabolism remain unclear. To explore this, we cultured STm in a medium using itaconate as the only
55 carbon source. Although initial growth was slow, STm adapted over time through mutations that
56 enhanced itaconate import and catabolism. We identified the genes required for growth on itaconate and
57 used metabolomics to reveal that itaconate causes widespread metabolic perturbations and high
58 oxidative stress. Our findings support itaconate degradation as a promising antimicrobial target and
59 define a medium suitable for screening potential inhibitors.

61 Introduction

62 *Salmonella enterica* serovar Typhimurium (STm) is a facultative intracellular pathogen that causes
63 gastroenteritis in humans, with the potential for systemic infection. It is the primary causative agent of
64 non-typhoidal *Salmonella* infections, with over 93 million cases and over 155 000 deaths yearly
65 worldwide, earning it a classification as a high priority pathogen by the WHO [1–4]. During infection,
66 STm survives in a diverse range of environments, including inside host macrophages, in specialized
67 compartments called *Salmonella*-containing vesicles (SCV) [5–7]. The SCV is a nutrient-limited, mildly
68 acidic (pH 4-5), and oxidative environment that STm has evolved to survive in, thanks in part to its
69 metabolic flexibility allowing the use of a variety of carbon sources [8]. While many studies have added
70 to our understanding of which metabolic pathways are used by intracellular STm both *in vivo* and *in*
71 *vitro*, the full picture remains incomplete [5–7]. To some degree, this is due to the heterogeneity of STm
72 physiology during infection, even when infecting the same tissue or cell type [9,10]. This localization of
73 bacteria during infection is of particular importance because it offers a protective environment from
74 some antibiotic treatments; owing to both limited accessibility by antibiotics with poor membrane-
75 permeability and the presence of slow growing STm populations that are resistant to treatment [10,11].
76 Nutrient starvation has been shown to be the primary cause of this protective phenotype, even when
77 compared to other stresses, such as acidic pH or oxidative stress, and can be attributed to the entire
78 population, not just a small subsect of highly-resistant persisters [10,12,13]. As such, recognizing how,
79 when, and why STm remodels its metabolism in response to nutrient limitation, will afford a better
80 understanding of why antibiotic treatments might fail and how to design new drugs targeting
81 intracellular infections [14].

82 Itaconate is an antibacterial and immunomodulatory molecule produced by activated
83 macrophages and pumped into the SCV at concentrations as high as 8 mM [15,16]. The antimicrobial

activity of itaconate is diverse; it can act as a non-covalent inhibitor, as well as a covalent modifier of cysteine residues in proteins through "*S*-itaconations", which can result in the inhibition of enzyme activity or modulation of protein function [17,18]. Over 1000 proteins in STm alone have been shown to be subject to *S*-itaconation, including enzymes involved in the TCA cycle (SDH: succinate dehydrogenase, SCS: succinyl-CoA synthetase) [19,20], in the glyoxylate shunt (Icl: isocitrate lyase) [21–23], and in *de novo* purine biosynthesis (PurF: amidophosphoribosyltransferase, GuaA: GMP synthetase, GuaB: IMP dehydrogenase, GuaC: GMP dehydrogenase) [24,25]. In response, STm and several other intracellular pathogens including *Pseudomonas aeruginosa* and *Mycobacterium tuberculosis* (Mtb), have evolved enzymes for itaconate detoxification [25–27]. The itaconate degradation pathway consists of three enzymes that convert itaconate into acetyl-CoA and pyruvate (**Fig 1**): itaconate CoA transferase (Ict), itaconyl-CoA hydratase (Ich), and citramalyl-CoA lyase (Ccl) [26]. The first step, involving the formation of itaconyl-CoA, has also been found to be catalyzed by other transferases or by SCS [28–31]. In STm, the three genes coding for the itaconate degradation enzymes are found within the same operon along with one other gene, *lgl*, which encodes a lactoylglutathione lyase involved in the detoxification of methylglyoxal [32–34]. Lgl is a secondary glyoxalase I enzyme, performing the same function as the canonical homolog in STm, GLO1, which is part of the methylglyoxal pathway along with GLO2. The full operon is referred to as the itaconate response operon (IRO) and is under the control of the LysR-family transcription factor, ItaR [35,36]. This is the first operon of *Salmonella* pathogenicity island (SPI)-13 [37,38], and the IRO is one of the most upregulated operons during STm invasion of macrophages [39–41]. Additionally, various studies have shown that deletion of IRO genes in STm, in the related Enteritidis and Gallinarum serovars, or in *Yersinia pestis,* resulted in attenuated infection of macrophages [32,37,40–43] and mice [32,44–48]. While the importance of the IRO for infection has been demonstrated, we lack a clear understanding of how

107 itaconate is used by STm during infection and the extent to which itaconate affects STm metabolism

108 among the other stressors found within the SCV.

109

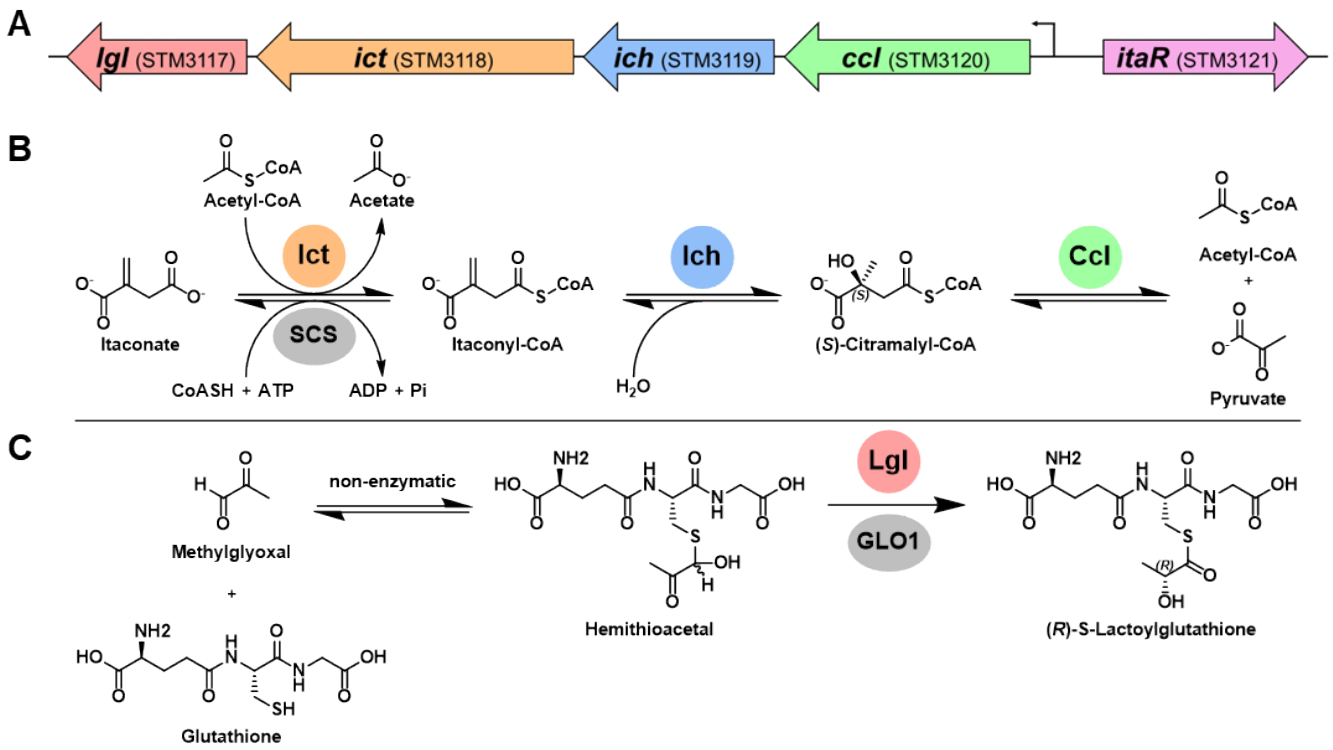

110

111 **Fig 1**: ***S*. Typhimurium itaconate and methylglyoxal detoxification by the enzymes of the itaconate**

112 **response operon (IRO).** (A) STm itaconate degradation enzymes (Ict, Ich, Ccl) are encoded on the SPI-

113 13 together with lactoylglutathione lyase (Lgl), under the control of the itaconate regulator protein

114 (ItaR). (B) Itaconate is degraded by three enzymes: Ict, Ich and Ccl. The action of Ict, a CoA-

115 transferase, can be replaced by that of succinyl-CoA synthetase (SCS). (C) Lgl detoxifies the toxic

116 metabolism byproduct methylglyoxal through isomerization of the spontaneously formed hemithioacetal

117 intermediate. This reaction can also be performed by glyoxalase I (GLO1).

118

119 To add to our understanding of the effects of itaconate on STm overall, we decided to study STm

120 growth on itaconate in axenic cultures using defined media. Expression of the IRO is not seen at any

121 stage of growth in LB, a nutrient-rich media, nor in response to infection-relevant stress factors (*e.g.,*
122 anaerobic, peroxide, nitric acid, bile shock), nor in other commonly used media that mimic the
123 intra-macrophage environment [49]. In fact, the IRO has only been shown to be expressed in response to
124 itaconate through ItaR activation [35,50,51]. As such, we chose to grow STm in the commonly used
125 M9-minimial media with itaconate as the sole carbon source, referred to as M9I herein. We compared
126 this with growth in the carbon-rich Mueller-Hinton broth (MHB), and another carbon-limited media, M9
127 with acetate as the sole carbon source (M9A). We found that STm growth in M9I is substantially slower
128 than in M9A or MHB, but that the rate can increase with subsequent subcultures to adapt to itaconate.
129 We identified two mutations that assist in this adaptation and used a metabolomics approach to map out
130 the dominant effects on STm metabolism. We also found that Ich, Ccl, and ItaR are necessary for
131 itaconate catabolism, but Ict is dispensable. In addition to improving our understanding of the interplay
132 between STm and itaconate, our results suggest that the use of M9I can mimic the intracellular
133 environment and could find application in the discovery of new antimicrobial molecules targeting
134 nutrient stress [14].

135 Results

136 ***1. STm growth on itaconate as a sole carbon source requires the ich, ccl, and itaR genes***

137 To develop conditions in which we could study the itaconate degradation pathway and in turn,
138 the effects of itaconate on STm, the bacterium was grown in M9I. STm can indeed grow in M9I, but at a
139 drastically reduced growth rate compared to rich media (**Fig 2A**) [52,53]. Subsequent subcultures
140 showed a consistent increase in the growth rate and OD at stationary phase. Comparing between the 2nd
141 and 6th subcultures, the doubling time decreased from 11 h to 3 h, yet it did not reach that observed in
142 MHB (0.4 h). The lag time decreased from ~90 h to ~40 h, compared to 1.8 h in MHB. Lastly, the
143 maximum OD_{600} at stationary phase shifted from 0.54 in the 2nd subculture to 1.7 in the 6th, compared to
144 2.5 in MHB.

145

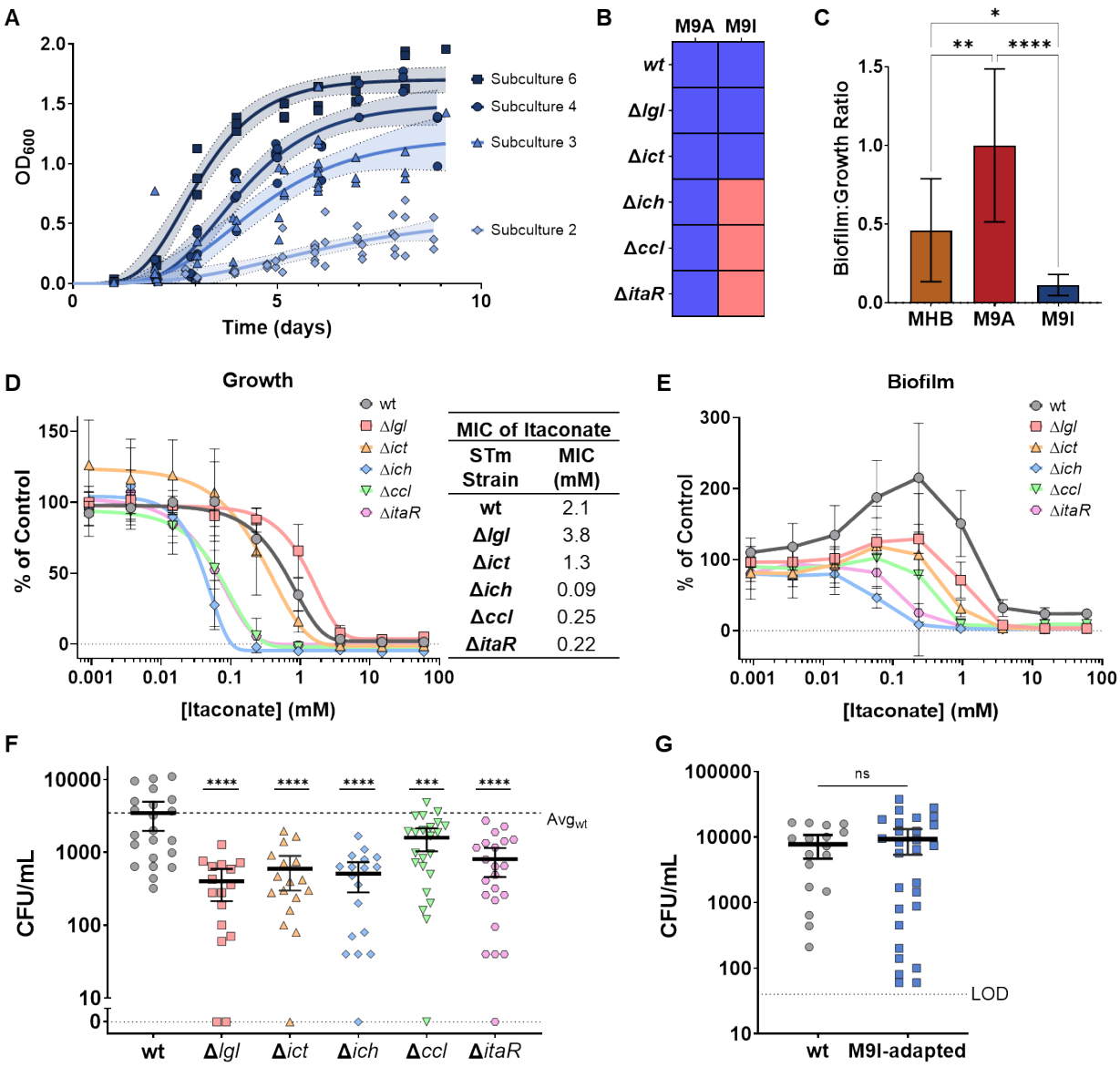

Fig 2: **STm can grow in media using itaconate as a sole carbon source.** (A) STm growth in M9I is initially slow, but after subsequent subcultures, it adapts and increases its growth rate. Logarithmic growth curves are shown with the bands denoting the standard error of each fit. (B) STm wt and IRO mutants grown in M9A and M9I, blue: growth and red: no growth. (C) Biofilm production by STm when grown in MHB, M9A, and M9I in 96-well plates. Biofilm was measured by crystal violet staining of the biomass, solubilizing and measuring the OD550. The measurements were normalized based on the planktonic growth (OD600) in each well. The data is given as a ratio of biofilm to planktonic

154 growth; n ≥ 8, one-way ANOVA (with Tukey's multiple comparisons test between groups). (D)
155 Itaconate MICs for each of the STm IRO mutants measured in M9A. Data is presented as the percentage
156 of growth (OD600) compared to the untreated control for each mutant, fit to a Gompertz MIC curve.
157 Error bars denote the SD; n = 4. The MICs are tabulated. (E) Biofilm levels produced in the same
158 itaconate MIC experiment as shown in D. The data is presented as a percentage of the amount of biofilm
159 produced by the untreated control, for each mutant. Straight lines are used to connect the datapoints. (F
160 and G) Intracellular survival of various STm mutants in RAW 264.7 macrophages, measured using a
161 gentamicin protection assay. STm wt was compared with (F) the IRO mutants or (G) M9I-adapted
162 STm. Error bars denote the 95 % CI of the mean. One-way ANOVA (with Dunnett's multiple
163 comparisons test with the wt) and two-tailed t-test used for comparing groups, respectively. All
164 experiments were repeated a minimum of 3 times. *, $p < 0.05$; **, $p < 0.01$; ***, $p < 0.001$; ****, $p <$
165 0.0001; ns, non-significant, $p > 0.05$.
166
167 To understand which genes in STm are required for the catabolism of itaconate, single-gene
168 deletion mutants of each of the IRO proteins were grown in M9I and compared with M9A as a negative
169 control (**Figs 2B and S1**). Growth was observed for all mutants in M9A, while only wt, Δ*lgl* and Δ*ict*
170 could grow in M9I. The cultures were left for 10 days without any visible growth for the Δ*ich*, Δ*ccl*, and
171 Δ*itaR* mutants. This establishes that the Ich and Ccl enzymes, as well as the transcription factor, ItaR,
172 are necessary for STm to degrade itaconate.
173
174 ***2. Biofilm production increases on acetate, but decreases on itaconate***
175 Bacteria such as *P. aeruginosa* [54] and *S. aureus* [55] have been shown to respond to itaconate
176 stress by increasing their production of biofilm. Thus, the amount of biofilm produced by STm when

177 grown in MHB, M9A, and M9I was measured by crystal violet staining (**Fig 2C**). STm cultures were
178 pre-adapted to the M9A or M9I media before measuring biofilm formation as described in the methods
179 section. Interestingly, compared to the MHB culture, biofilm production was substantially increased in
180 M9A, but decreased in M9I. An explanation for this is proposed later.
181
182 ***3. An inactive itaconate degradation pathway increases susceptibility to itaconate***
183 STm has numerous mechanisms to respond to dicarboxylic acid stress, with the itaconate
184 degradation pathway being the most direct one. To assess the effect that itaconate degradation has on the
185 ability of STm to tolerate itaconate, we measured the MIC of itaconate for STm grown in M9A – a
186 media in which the glyoxylate pathway and Icl (one of the enzyme targets of itaconate) are necessary.
187 Consistent with the growth results presented in **Fig 2B**, the Δ*ich*, Δ*ccl*, and Δ*itaR* mutants (MIC of 0.09,
188 0.25, and 0.22 mM, respectively) were approximately an order of magnitude more susceptible to
189 itaconate than wt STm or mutants Δ*lgl* and Δ*ict* (2.1, 3.8, and 1.3 mM, respectively; **Fig 2D**). Next,
190 biofilm production was measured in response to itaconate treatment in M9A medium to see if STm and
191 the IRO mutants exhibit any stimulation of biofilm production when itaconate is used as an antibiotic,
192 rather than a carbon source. Indeed, wt STm was found to exhibit a large increase in biofilm at sub-MIC
193 concentrations of itaconate, reaching a peak at ~230 μM (**Fig 2E**). The biofilm response was dampened,
194 though still observed, for Δ*lgl,* Δ*ict*, and Δ*ccl,* with the peak amount of biofilm being produced at ~60
195 μM itaconate. Both the Δ*ich* and Δ*itaR* mutants did not appear to exhibit an increase in biofilm
196 production at any concentration of itaconate. This suggests that having an intact itaconate degradation
197 pathway—the resistance mechanism for the antibiotic being used here—is necessary to induce biofilm
198 stimulation in response to itaconate.
199

200 ***4. STm IRO mutants are attenuated in their ability to infect macrophages***

201 STm IRO mutants were previously shown to be attenuated in their ability to infect macrophages
202 in screens of deletion mutant libraries [37,40–43]. These results were successfully reproduced by
203 comparing each of the STm mutants in a gentamicin protection assay (in which the extracellular bacteria
204 are selectively killed by gentamicin) using RAW 264.7 murine macrophages (**Fig 2F**). When compared
205 to wt STm, all five mutants showed significantly attenuated intra-macrophage proliferation after an
206 infection period of 20 h. Interestingly, the trends observed in the ability of different mutants to
207 metabolize/resist itaconate did not translate to this experiment (see **Fig 2D**). Whereas wt STm had an
208 average infection of 3500 CFU/mL, Δ*lgl* (400 CFU/mL) was the most attenuated, followed by Δ*ich* (510
209 CFU/mL), Δ*ict* (600 CFU/mL), Δ*itaR* (810 CFU/mL), and Δ*ccl* (1600 CFU/mL). Furthermore, the
210 attenuation of Δ*ich* was observed 1 h after infection, after which the CFU was maintained over 72 h (**S2**
211 **Fig**). This seems to indicate that the diminished infection relates to an inability to colonize the
212 macrophages.

213

214 ***5. Mutations in rpoS and dctA benefit growth on itaconate***

215 To explore the ways in which STm adapts to more efficiently catabolize itaconate and improve
216 its growth in M9I over subsequent subcultures, we sequenced the M9I-adapted and M9A-adapted STm
217 strains. The same STm parent strain (cultured once in nutrient broth, NB) was subcultured three times in
218 parallel in M9I and M9A. The dominant background mutations that were observed in the culture prior to
219 M9I/A-adaptation (*i.e.* background differences between this parent strain and the ATCC 14028 reference
220 genome) are listed in **Table S1**, and were filtered out before the following analysis of mutations
221 identified in M9A and M9I. Across three replicates in each medium, 44 distinct mutations were
222 observed for growth in M9A, with only six detected in all replicates (**S3A Fig**). Notably, none of the

223 mutations found in the M9A-adapted strains were observed at a frequency above 25% and hence may
224 not have conferred significant growth advantages. In the M9I cultures, 81 distinct mutations were noted,
225 with an overlap of five genes across all replicates (S3B Fig). Further inspection of these mutations
226 revealed that three of those five genes were also found to be mutated in the parent strain, but at different
227 residues, and were also not found at frequencies above 25%. As such, those mutations could not be
228 confidently linked to improved growth in M9I. The mutations identified in the remaining two genes
229 were uniquely found in the M9I-adapted strains, in all three replicates, and were mutated in frequencies
230 above 25% in at least one replicate. Thus, these likely conferred an advantage to growth in M9I (**Table**
231 **1**). The most abundant set of mutations were single nucleotide polymorphisms (SNPs) that introduced a
232 stop codon into the gene of the alternative RNA polymerase sigma factor, *rpoS*. RpoS regulates a large
233 group of genes during entry into stationary phase and as part of the general stress response of STm and
234 other γ-proteobacteria, including a response to temperature, pH, osmolarity and oxidative stress [56].
235 Furthermore, RpoS has been established as an important virulence factor [57,58]. Four distinct nonsense
236 mutations were observed across the three growth replicates at varying frequencies. If we presume that
237 each bacterium contains only one of these SNPs, 95-100 % of each culture no longer had a functional
238 RpoS. This strongly suggests that RpoS is a hindrance to growth in M9I.
239

240 **Table 1**: **Significant STm genomic mutations during adaptation to M9I.**

Gene	Replicate	Mutation[a]	Type	Frequency[b]	Description
rpoS	1	W148X (TGG→TAG)	Nonsense	67.7%	RNA polymerase sigma factor RpoS
		E132X (GAG→TAG)	Nonsense	14.5%	
		L234X (TTG→TAG)	Nonsense	13.2%	
	2	W148X (TGG→TAG)	Nonsense	100%	
	3	Q251X (CAA→TAA)	Nonsense	92.7%	
		E132X (GAG→TAG)	Nonsense	5.7%	
pdeK / *dctA*	1	intergenic (+130/-28) (C→T)	SNP	16.3%	**PdeK**: Putative cyclic di-GMP phosphodiesterase
		intergenic (+92/-66) (+T)	Insertion	15.4%	
		intergenic (+92/-66) (+A)	Insertion	15.4%	
	2	intergenic (+136/-22) (G→T)	SNP	69.6%	
		intergenic (+130/-28) (C→T)	SNP	29.1%	

	3	intergenic (+130/-28) (C→T)	SNP	7.3%	**DctA**: Aerobic C4-dicarboxylate transport protein

241 [a] Colour coding highlight where the exact same mutation is observed in more than one replicate. [b] The
242 significance threshold was set at >25% frequency for at least one mutation within the three replicates
243 and for mutations not also observed in M9A-adaptated strains.
244
245 The second most abundant set of mutations were found in the intergenic region between the
246 *pdeK* and *dctA* genes, upstream of *dctA* (**Fig 3**). PdeK is a putative cyclic di-GMP phosphodiesterase
247 and DctA is an aerobic C4-dicarboxylate transport protein involved in importing molecules such as
248 succinate, fumarate and malate into the cell [59]. Four mutations were identified in total, consisting of
249 two distinct insertions (either A or T) directly before the -10 element of the promoter, and two SNPs in
250 the 5'-UTR region of *dctA*, at an IscR transcription factor binding site [60]. One of the SNPs (C→T,
251 +130/-28) was found in all three replicates, between 7-30 % frequency, while the other SNP (G→T,
252 +136/-22) was found in only one replicate, although at the highest frequency (70%) among all replicates
253 for this locus. Both insertion mutations were found in the same replicate at 15 % frequency. Based on
254 their frequencies, the mutations in the *pdeK*/*dctA* intergenic region have a lesser impact compared to
255 those of the *rpoS* SNPs, however, it is possible that over a few extra subcultures, higher frequencies in
256 the *pdeK*/*dctA* mutations would arise. Taken together, these mutations in the *dctA* promoter region likely
257 affect transcription levels. Based on previous studies identifying similar mutations [60,61] that are
258 discussed later, we suggest that these result in higher expression levels of *dctA*, and increased transport
259 of itaconate inside the cell.
260

Fig 3: **Mutations acquired selectively during growth in M9I that are found in the intergenic regions between *pdeK* and *dctA*.** The two SNPs and two insertion mutations that were observed and descripted in Table 1 are in purple. Relevant transcription factor binding sites and promoter regions are annotated. Nucleotides denoted by a green * refer to sites for which mutations were previously characterized by Amin *et al.* (2022) [62] in the CRP binding region, or Quandt *et al.* (2014) [61] and Wenner *et al.* (2024) [60] in the IscR binding region, and that resulted in increased *dctA* expression and improved growth on C_4-dicarboxylates. CRP: cAMP receptor protein, TSS: transcription start site, S.D.: Shine-Dalgarno sequence.

Given that RpoS is an important regulator of virulence for STm, the ability of M9I-adapted STm to infect macrophages was investigated. Previously, Δ*rpoS* mutants have been shown to have little to no attenuation in their ability to infect macrophages, but were attenuated in mice models [63]. To confirm this phenotype, and determine if the other mutations factored in, proliferation of the wt and M9I-adapted STm were compared in RAW 264.7 macrophages (**Fig 2G**). Indeed, no significant difference between the means of the two strains was observed. The wt STm burden was 7700 ± 3100 (95% CI) CFU/mL and the burden of the M9I-adapted strain was 9300 ± 3900 (95% CI) CFU/mL. Altogether, this suggests that the mutations acquired to improve itaconate catabolism do not affect the ability of STm to infect macrophages.

280

281 ***6. Remodeling of STm metabolism when grown on itaconate***

282 To gain further insight into the general adaptations of STm to itaconate, a LC-MS-based targeted
283 metabolomic analysis was performed. The metabolism of STm was compared at both a mid-exponential
284 phase (EP) and at an early-stationary phase (SP) of growth in MHB, M9A, and M9I. STm growth curves
285 were first reestablished under the larger-scale conditions used for the metabolomics experiment to
286 appropriately determine the OD at the EP and SP endpoints. (**Fig 4A**). The detection methods used were
287 optimized to search for a panel of 296 ions in total, and overall, 129 ions were quantified and included in
288 the analysis. Principal component analysis (PCA) revealed that the metabolic profiles of STm grown in
289 each medium differed considerably, while the profiles at different stages of growth (EP versus SP)
290 within each medium were more similar (**Fig 4B**). The M9I EP and SP profiles completely overlapped,
291 while only one M9A SP sample fell outside of the EP 95 % confidence region. The largest difference
292 between growth phase profiles was seen by STm grown in MHB, although the difference was small
293 compared to the profile differences between media. The significance of metabolite differences across all
294 conditions were determined by two-way ANOVA, summarized here as a heatmap showing the relative
295 abundances of the 40 most significant (ranked by p-value) metabolites (**Fig 4C**). An examination of the
296 pathway ontology revealed that the nucleotide and carbohydrate metabolic pathways were the most
297 abundant among significant features (**Fig 4D**). A secondary analysis consisting of pairwise comparisons
298 (T-tests) between media conditions (stratified by growth phase) was also done to identify the specific
299 fold changes (FC) in significant ($\log_{10}(FC) > 2$ and p-value < 0.05) metabolites across the different
300 condition sets (**S4A Fig**). Multiple pathway enrichment analysis using both the ANOVA and T-test/FC
301 identified significant metabolites and were used to guide our understanding of these results (**S4B-D Fig**).
302 However, no specific pathways were found to be markedly ($p < 0.05$) enriched by this method, which

appears to indicate that the effects across the three media are on the STm metabolism as a whole. As such, the pathways most abundant in significant metabolites, as determined by two-way ANOVA across all six conditions, were prioritized for analysis since they could give a clearer picture of metabolic differences across the three media.

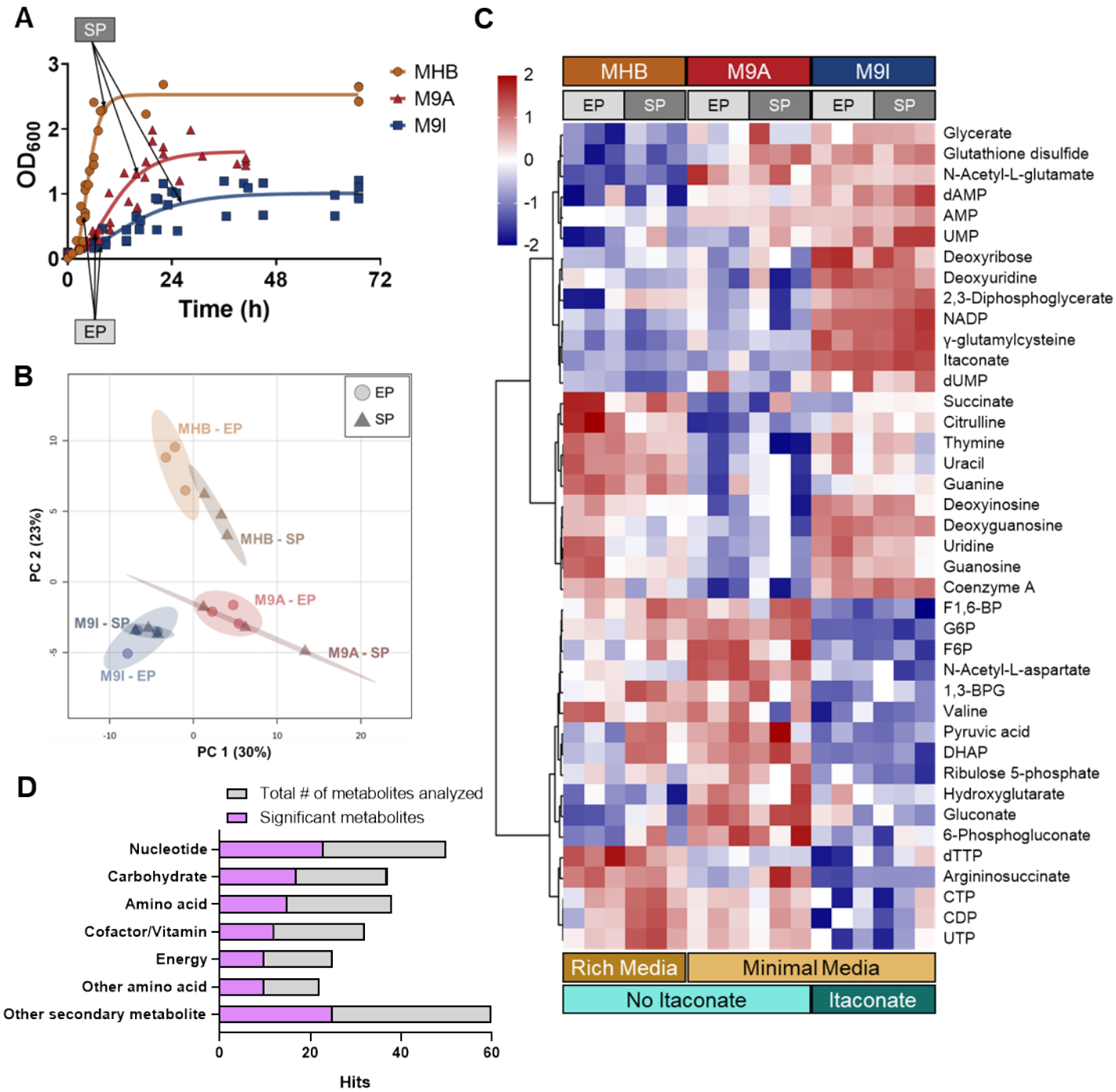

308 **Fig 4**: **Metabolomics of STm in MHB, M9A, and M9I at two phases of growth.** (A) Growth curves
309 in each medium under the culture conditions used for metabolomics with the mid-exponential phase
310 (EP) and early-stationary phase (SP) identified. (B) Principle-component analysis of all six conditions.
311 Ellipses indicate 95% CI, n = 3 per condition. (C) Heat map showing the normalized abundance of each
312 of the most significant metabolites as identified by a two-way ANOVA (ranked by p-value and using
313 Ward's method to cluster features). (D) Pathway ontology analysis showing both the total number of
314 metabolites measured by our HPLC-MS method and those that are significant in each pathway.
315
316 ***i) Effects on carbon metabolism.*** When growing on non-glycolytic carbon sources such as
317 acetate or succinate, STm and other enteric bacteria rely on gluconeogenesis for the anabolic production
318 of the various sugars necessary for growth and cellular functions, such as cell wall and nucleotide
319 biosynthesis [64–66]. In M9A, the metabolomics analysis reveals an abundance of gluconeogenic
320 metabolites, as well as pentose phosphate pathway (PPP) sugars, consistent with active growth (**Fig 5**).
321 However, when grown on itaconate, the opposite trend is observed, with a broad and drastic decrease in
322 metabolites within the glycolysis/gluconeogenesis and PPP pathways. Given that itaconate enters carbon
323 metabolism in the form of acetyl-CoA and pyruvate after being degraded, a similar need for
324 gluconeogenesis would be expected when growing in M9I. The reduced flux in this pathway could be a
325 factor in the substantially reduced growth rates of STm in M9I.
326

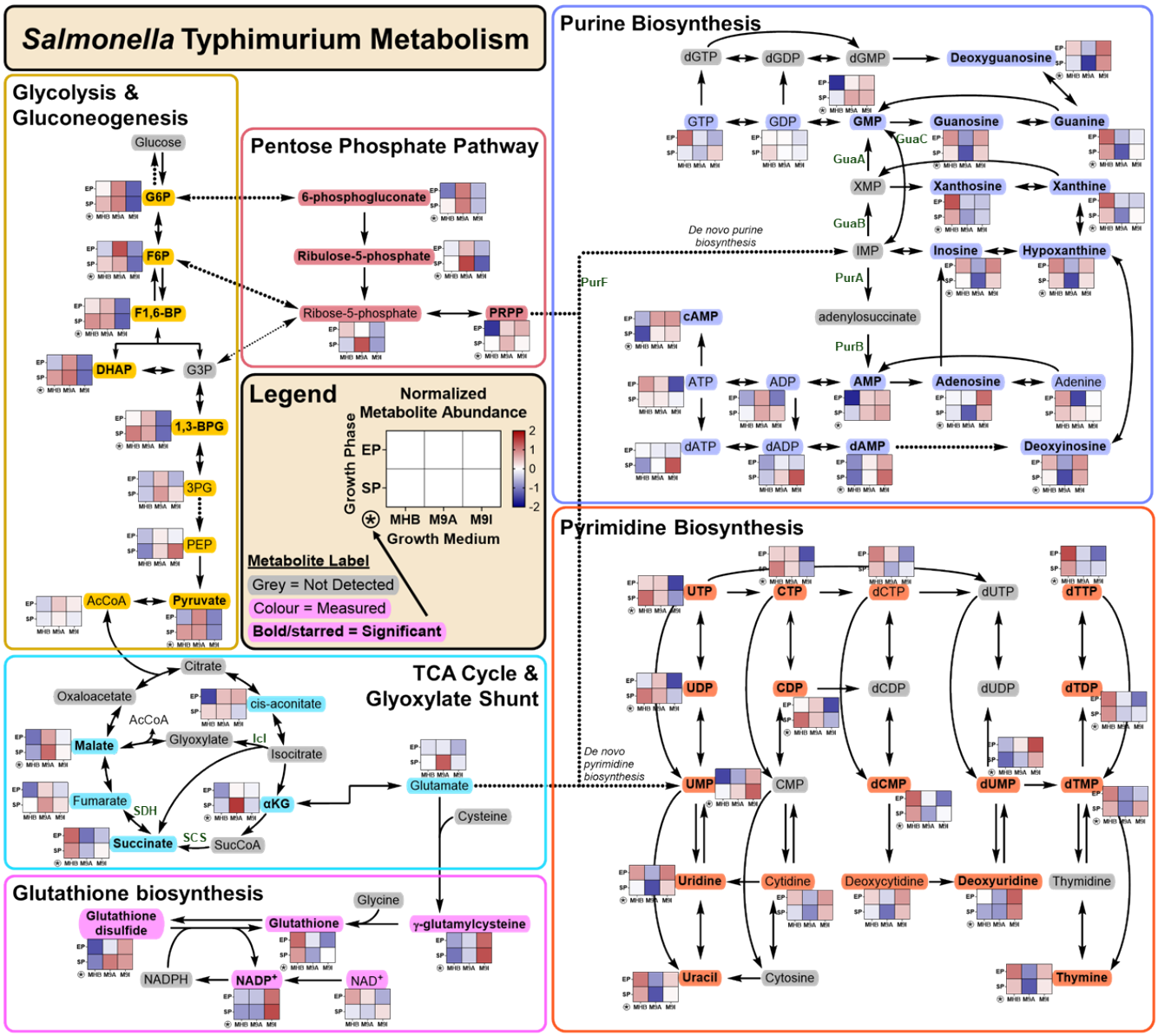

Fig 5: **Pathway analysis of STm metabolomic results.** Relative metabolite abundances across the three media (MHB, M9A, M9I) and two growth phases (EP and SP) are shown as a single heatmap for selected metabolites quantified in our method and placed adjacent to the molecule in the pathways. Double sided arrows indicate reversible reactions performed by the same enzyme, double arrows in opposite directions indicate reversible processes that are performed by different enzymes. Dotted lines indicate multiple enzymatic steps. G6P: glucose-6-phosphate, F6P: fructose-6-phosphate, F1,6-BP: fructose-1,6-bisphosphate, DHAP: dihydroxyacetone-phosphate, G3P: glyceraldehyde-3-phosphate,

335 1,3-BPG: 1,3-bisphosphoglycerate, 3PG: 3-phosphoglycerate, PEP: phosphoenolpyruvate, AcCoA:
336 acetyl-CoA, PRPP: 5-phosphoribosyl-1-pyrophosphate, αKG: α-ketoglutarate, SucCoA: succinyl-CoA.
337
338 For the TCA cycle, our results are less clear because no significant accumulation or depletion of
339 any detected TCA metabolite is seen for STm in M9I. Itaconate is a known inhibitor of at least three
340 enzymes in the STm TCA and glyoxylate cycles: Icl, SDH, and SCS. Inhibition of Icl cannot be
341 confidently established because isocitrate could not be measured. However, the slight increase in
342 abundance of cis-aconitate during the M9I exponential phase is consistent with Icl inhibition. This is
343 similarly the case for SCS, which converts SucCoA to succinate; SucCoA was not measured, and little
344 information can be gleaned from the levels of α-ketoglutarate (one metabolite before SCS) in M9I.
345 Furthermore, the lack of succinate accumulation suggests that any SDH inhibition is not affecting the
346 flux through this part of the cycle compared to the two other media. In M9A, the observed accumulation
347 of malate could indicate activity through the glyoxylate cycle, which is important for growth on acetate
348 [67].
349
350 ***ii) Effects on glutathione metabolism.*** Exposure to electrophilic compounds, such as itaconate,
351 is known to induce specialized electrophilic stress responses [68]. Glutathione (GSH) is an antioxidant
352 that is often employed in response to electrophilic and oxidative stress. In the case of itaconate, it has
353 been shown to form adducts through thia-Michael addition to itaconate [69]. By comparing GSH levels
354 to those of its oxidized pair, glutathione disulfide (GSSG), we can infer the oxidative state of the cells
355 under each condition (**Fig 5**). When growing on itaconate, the GSH to GSSG ratio strongly favours the
356 oxidized form. This is true also for growth in M9A at stationary phase, but the ratio is flipped in MHB,
357 indicating little or no oxidative stress in this rich media. In M9I, we also see an abundance of the

358 glutathione precursor γ-glutamylcysteine, which may indicate a general upregulation of glutathione
359 production in response to this stress. Similarly, $NADP^+$, the oxidized form in the $NADP^+$/NADPH
360 redox pair required by enzymes for cycling between GSH and GSSG, is also found in relatively large
361 quantities in M9I compared to both MHB and M9A. Although it is difficult to draw conclusions from
362 the $NADP^+$ abundance alone, the high amounts detected support the observation of elevated oxidative
363 stress in M9I, with NADPH recycling being slower than GSSG formation.
364
365 ***iii) Effects on nucleotide biosynthesis.*** Given that nucleotide biosynthesis was the most
366 represented pathway in our data and that recently, itaconate was found to affect the *de novo* biosynthesis
367 of purines in STm [24] and Mtb [25], the effects of itaconate on purine and pyrimidine biosynthesis
368 were explored (**Figure 5**). To our discontent, the molecules involved in *de novo* purine biosynthesis
369 were not detected, thus limiting our ability to compare with previous results. Nonetheless, trends in the
370 broader metabolic profiles for the pathways downstream of the *de novo* portion of purine and pyrimidine
371 biosynthesis were identified. The previous work had observed decreases in the end products of *de novo*
372 purine biosynthesis (IMP, AMP, and GMP) in response to itaconate treatment through inhibition of the
373 first step in the pathway, PurF, and the GuaABC enzymes in GMP biosynthesis [24,25]. The data
374 presented here shows that the GMP and AMP levels are not depleted for cultures in M9I, and are at
375 similar levels in M9A, whereas the levels were considerably lower in MHB. Considering that we are
376 analyzing the metabolomes of media-adapted STm that have established a new homeostasis and growth
377 rate within each media (compared to experiments in which itaconate exposure is a treatment group), it
378 follows that we are likely not to observe the same responses as in prior studies.
379 Broadly, in M9I, we observe a depletion in the supply of both purine and pyrimidine nucleotide
380 di- and triphosphates that is particularly prominent in the exponential phase compared to stationary. This

381 could indicate a general lack in energy supply, or a lag in the ability of STm to replenish nucleotide
382 triphosphate stores needed for transcription at a pace that matches the growth rate in this phase. In the
383 case of deoxynucleotides, we see an accumulation of all three species of adenine phosphate (dAMP,
384 dADP and dATP) in the stationary phase. For the pyrimidine deoxynucleotides, we generally see lower
385 quantities of these species in M9I, however the trend of abundance increasing from EP to SP remains.
386 This accumulation in SP could be the result of a reduced ability to downregulate the synthesis of
387 deoxynucleotides in M9I once the cells stop actively growing. Furthermore, we see increased levels of
388 purine and pyrimidine deoxynucleosides and some nucleosides in M9I, especially when compared to
389 M9A for which a general deficit of these species is observed. This could be related to usage of the
390 salvage pathways. *De novo* purine and pyrimidine biosynthesis stems from the metabolite
391 phosphoribosyl diphosphate (PRPP) in the PPP. Given the higher flux through PPP that we observed in
392 M9A, STm may be better able to rely on *de novo* biosynthesis of nucleotides under these conditions.
393 However, in M9I, given the lack of gluconeogenesis observed, the bacteria may rely more on the
394 salvage pathways for their nucleotides.

395 Another metabolite of interest is cyclic-AMP (cAMP), which is a secondary signalling molecule
396 that regulates transcription through the cAMP receptor protein (CRP) in response to changes in carbon
397 source, especially in the absence of glucose [70]. As expected, a higher abundance of cAMP was seen in
398 both M9I and M9A compared to MHB.

400 Discussion

401 We have shown that STm can grow on itaconate as a sole carbon source, and that growth rates
402 on itaconate increase with subculturing. Itaconate degradation requires Ich, Ccl, and the IRO regulator
403 ItaR to accomplish this. The first enzyme in the itaconate degradation pathway, Ict, is dispensable,
404 although the growth of STm Δ*ict* in M9I is still attenuated. Similarly, the other enzyme in the IRO, Lgl,
405 was not required for itaconate degradation, as expected given its function in methylglyoxal
406 detoxification. These findings correlate with itaconate susceptibility in M9A, in which a ~10-fold
407 decrease in MIC was observed for STm mutants lacking one of the three required IRO genes compared.
408 This is the first report identifying the genes of the STm IRO that are necessary for itaconate degradation,
409 and is consistent with prior work on itaconate degradation in *P. aeruginosa*. In *P. aeruginosa* Ich and
410 Ccl are required for growth on itaconate [20,71–73], with some groups reporting that Ict deletion
411 prevents growth up to 24 h [20,54] or 36 h [72], while another saw attenuated growth after 36 h in a
412 *Pseudomonas putida* strain heterologously expressing the *P. aeruginosa* IRO [71]. It may be that *P.*
413 *putida,* and not *P. aeruginosa,* has an Ict alternative (as seen with STm) that allows growth without Ict.
414 However, longer growths of Δ*ict P. aeruginosa* on itaconate are needed to confirm this. To our
415 knowledge, *P. aeruginosa itaR* deletions mutants have not been tested in their ability to degrade
416 itaconate. Furthermore, we were able to corroborate previous work showing that each single gene
417 deletion mutant of the STm IRO genes results in a reduced ability to infect macrophages, regardless of
418 their necessity for degradation [37,40–43].

419 The extended lag phase observed in M9I and subsequent adaptation to the M9I media seem to
420 indicate that itaconate is not a preferred carbon source for STm under these conditions. The nonsense
421 mutations introduced into *rpoS* to near fixation after only three subcultures is indicative of an
422 RpoS-induced inhibition of itaconate catabolism, uptake, or otherwise. RpoS is a generalized stress

423 response and a stationary phase sigma factor that competes with the primary sigma factor RpoD and
424 others for the core RNA-polymerase [56]. As such, high RpoS levels results in reduced growth through
425 RpoD competition. When this is detrimental to bacteria, RpoS mutations are frequently selected for to
426 correct this through antagonistic pleiotropy, which is often reversible [74,75]. Our finding that M9I
427 adaptation did not affect STm infection of macrophages is consistent with the previous finding that *rpoS*
428 deletion does not affect infection or survivability in macrophages *in vitro* [63]. Furthermore, RpoS has
429 been linked to biofilm formation through multiple transcription regulators [76–78]. The observed
430 increased baseline biofilm levels between cultures in M9A compared with M9I—along with the fact that
431 wt STm grown in M9A is stimulated to produce excess biofilm by sub-MIC concentrations of
432 itaconate—leads us to believe that the *rpoS* mutations are a factor in the reduced biofilm production
433 phenotype observed in M9I growth. Biofilm production when grown on non-glycolytic carbon sources is
434 supported by gluconeogenesis [79]. As such, we can correlate the higher biofilm levels in M9A and the
435 lower levels in M9I, with their respective increase and decrease in metabolic flux through
436 gluconeogenesis and PPP observed in our metabolomics results.

437 A reduction in biofilm stimulation at sub-MICs of itaconate was also detected for the IRO
438 mutants, particularly those incapable of degrading itaconate. The sub-MIC biofilm stimulatory response
439 is common among biofilm-forming bacteria as part of their stress response to antibiotic treatment, with
440 some differences observed between classes of antibiotics [80]. Recently, in *E. coli,* this phenomena has
441 been directly linked with global changes in central metabolism and respiration in response to antibiotic
442 treatment [81]. Yaeger *et al.* [81] showed that knockout mutants of the TCA cycle (among others) have
443 a hampered biofilm stimulation response to sub-MIC antibiotic stress. Given that itaconate directly
444 inhibits multiple enzymes in the TCA cycle, it follows that limiting/eliminating the ability of STm to
445 detoxify itaconate in the knockouts results in more TCA cycle inhibition and a similar decrease in

446 biofilm production as seen with the *E. coli* TCA-cycle mutants. The observation of STm Δ*lgl* reduced
447 biofilm formation can be included in this hypothesis through a reduced ability to handle
448 itaconate-induced oxidative stress via reduced methylglyoxal detoxification and its downstream effects
449 [33]. Complicating this hypothesis is a study that looked at itaconate treatment of STm in LB cultures, in
450 which they did not observe any sub-MIC increase in biofilm production [82]. This will require further
451 investigation to properly understand the STm biofilm response to itaconate treatment, how growth on
452 different carbon sources affects it, and how it relates to the biofilm stimulation by itaconate seen in other
453 species [54,55].

454 Various C_4-dicarboxylates (C4DCs; *e.g.* succinate, fumarate, L-aspartate) are taken up and used
455 by STm and other enteric pathogens as carbon sources or signaling molecules at various stages of
456 infection [83,84]. A key example is succinate, a structural analog of itaconate, which is used by STm to
457 fuel its growth during infection of the gut, where succinate is produced by the host microbiota [85].
458 However, during infection of macrophages, STm uses glucose and other glycolytic intermediates as a
459 preferred carbon source over succinate [60,86–88]. This is despite the fact that macrophages accumulate
460 succinate during infection due to a shift in the host cell metabolism from oxidative phosphorylation to
461 glycolysis [86,89]. Instead, this succinate is recognized by *Salmonella* as a molecular signal to induce
462 virulence genes important for intracellular survival through expression of SPI-2 [90]. Succinate and
463 other C4DCs are taken up aerobically by the DctA transporter and anaerobically by DcuB [84,91]. DctA
464 has also been shown to be sufficient for itaconate transport [92]. RpoS has been reported to restrict STm
465 uptake and catabolism of C4DCs through indirect repression of *dctA* [60,93], and direct repression of
466 TCA cycle genes used for C4DC catabolism [94,95]. STm growth on succinate exhibits an extended lag
467 phase, even compared to other enteric bacteria like *E. coli*, and deletion of *rpoS* was also shown to
468 substantially shorten the lag phase [93]. In light of this, we can reasonably conclude that *rpoS*

469 suppression of itaconate uptake and metabolism genes is the reason for the rapid selection of
470 non-functional *rpoS* mutants during growth in M9I.

471 The mutations observed in the *dctA* promoter region are also consistent with our understanding
472 of *dctA* regulation through both RpoS and non-RpoS mechanisms. In fact, the transcriptional regulation
473 of *dctA* is known to be controlled directly by at least three transcription factors: the membrane-bound
474 DcuS-DcuR two-component system, the cAMP receptor protein (CRP), and the iron sensing regulatory
475 protein, IscR (**Fig 3**) [60,83,91]. CRP senses cAMP increases under carbon-limiting conditions, leading
476 to induction of many genes, including *dctA* [70]. It is also responsible for catabolite repression of *dctA*
477 expression when preferred (*i.e.* glycolytic) carbon sources are available. Recently, a SNP in the
478 CRP-binding site of the STm *dctA* promoter region was reported to increase CRP induction of DctA,
479 allowing growth on normally non-permissibly low orotate concentrations (which is also transported by
480 DctA) [62]. On the other hand, IscR represses *dctA* expression and inhibits growth on succinate [60].
481 Previously, in two separate studies, a total of three SNPs in the IscR binding site of the *dctA* 5'-UTR
482 resulted in reduced IscR-mediated repression, increased *dctA* expression, and an improved ability of
483 both STm and *E. coli* to grow on succinate or other C4DCs [60,61]. To our satisfaction, both of the
484 SNPs identified here through M9I-adaptation coincided with those previously discovered. The C→T
485 (+130/-28) mutation is the exact same as that found by Wenner *et al.*,[60] and the G→T (+136/-22) SNP
486 involves the same G nucleotide reported by Quandt *et al.* [61], although they observed a transition to an
487 A, and we observed a transversion to a T. In reference to the A or T insertion observed immediately
488 upstream of the *dctA* -10 element in our study, it has been shown that STm RpoD has a higher tolerance
489 for an "extended" -10 element compared to *E. coli* [96]. These results suggest that this last mutation may
490 result in a positive, if not neutral, effect on RpoD binding to promote *dctA* expression. In summary, both
491 sets of mutations acquired during M9I-adaptation are expected to translate into an improved ability of

492 STm to uptake itaconate through DctA and a reduced suppression of the TCA cycle genes necessary for
493 growth on C4DCs.

494 Recalling that many proteins have been identified as targets of *S*-itaconation, it was interesting to
495 not find any mutations in our genotyping results for cysteines to another amino acid. While we would
496 not expect active site cysteine residues of enzymes to be mutated, any instances of negative allosteric
497 effects due to *S*-itaconation would be a possible site for mutation to prevent that. However, even when
498 looking at the low frequency mutations, there were only 2 instances of cysteines being mutated to
499 another amino acid, while in 8 cases, cysteines were gained. This finding suggests that in STm, most
500 *S*-itaconation sites that are not in an enzyme active site may have a neutral or positive effect on enzyme
501 function, such that mutation of the cysteines was not beneficial to the cells during growth on itaconate.
502 This is consistent with the fact that in prokaryotes, all the validated targets of *S*-itaconation inhibition
503 have been within enzyme active sites [18], whereas in eukaryotic cells, there are many instances of
504 *S*-itaconations at regulatory sites resulting in altered protein functions. Alternatively, it could be that
505 STm employs inducible protective strategies to sufficiently protect reactive cysteines, whether through
506 glutathione-mediated protection or other unexplored mechanisms. For example, *S. aureus* has been
507 shown to employ reversible *S*-bacillithiolations of protein cysteines in response to itaconate- and
508 succinate-induced stress. However, STm is not known to make bacillithiol.

509 In light of the mutational adaptations uncovered herein, it is crucial to consider the potentially
510 far-reaching effects that these may have when interpreting metabolomic results. Without an RpoS stress
511 response, STm must rely on non-RpoS mechanisms to manage the stress of prolonged exposure to
512 itaconate during growth in M9I. A key indicator of this stress was the increased flux through the
513 glutathione metabolism pathway. Higher levels of both γ-glutamylcysteine and GSSG, point towards a
514 greater need for glutathione during growth on itaconate. The lower levels of GSH detected in M9I

515 compared to the other media are likely due to the sequestration of GSH as oxidized derivatives. It is
516 known that GSH can form adducts with itaconate in mammalian cells as a means of buffering
517 electrophilic stress [69]. This has been seen with fumarate, as well, with the fumarate-GSH adducts
518 being recycled by glutathione reductase, the enzyme that uses NADPH to reduce GSSG back into GSH
519 [97,98]. However, no such recycling pathway for itaconate-GSH adducts has been identified. It is
520 possible that there is a population of itaconate-GSH adducts that accumulates in bacteria, and more
521 research will be needed to explore the presence of these adducts in STm and whether the cells are able to
522 recycle the adducts. A similar phenomenon was seen with STm during exposure to peroxide in glucose-
523 rich medium that resulted in excess production of methylglyoxal [99]. Activation of the methylglyoxal
524 detoxification pathway created a glutathione sink, reducing the available GSH levels. Interestingly, this
525 connects Lgl activity as a homolog of GLO1 with the rest of the IRO, both of which respond to different
526 aspects of oxidative stress found in the SCV.

527 Previous studies have explored the effect of itaconate on the metabolism of various bacteria
528 when grown in rich media including *E. coli* (grown in LB) [82], Mtb (7H9) [25], *P. aeruginosa* (LB)
529 [20], *V. cholerae* (LB) [100], and *S. aureus* (RPMI or MHB) [101,102]. In each study, flux through the
530 TCA cycle was highlighted, with observations generally consistent with the known targets of itaconate
531 inhibition. These studies carry the context that they were evaluating growth disruption by itaconate in
532 carbon-rich media. As such, our results are distinguished from these by exploring the overall impact on
533 STm metabolism and for STm growing on itaconate, rather than the ways in which it affects the
534 metabolism of other carbon sources.

535 Of note, *P. aeruginosa* was shown to be able to efficiently catabolize itaconate, incorporate it
536 into its central metabolism and utilize it for biofilm production through gluconeogenesis [20]. This is
537 consistent with the fact that *P. aeruginosa* has a different itaconate degradation pathway from STm [26]

538 and more readily proliferates on itaconate as a sole carbon source [20,54,72]. In addition to the low
539 homology between *P. aeruginosa* Ict/Ich enzymes and those of STm [26], *P. aeruginosa* also has a
540 dedicated itaconate transporter found within its IRO. This transporter was reported to be necessary for
541 efficient growth on itaconate [71–73]. This can be contrasted with our findings that STm required
542 mutations to increase DctA transporter expression, and elimination of RpoS-induced repression of
543 C4DC usage in central metabolism. Taken together, it appears that *P. aeruginosa* is better equipped for
544 use of itaconate as a carbon source compared to STm and likely other species with homologous IROs.
545 The full extent to which *Salmonella* uses itaconate as a carbon source or molecular signal during
546 infection is highly relevant to the development of antibiotics that target intracellular bacteria. Herein,
547 more light is shed on this important phenomenon. STm exhibits an extended lag phase and extremely
548 slow growth rate in M9I that is ameliorated by rendering it RpoS non-functional and increasing
549 itaconate uptake via augmented DctA expression. This is paralleled by STm use of succinate as a carbon
550 source, for which slow axenic growth is improved through deletion of *rpoS* or introduction of mutations
551 that improve DctA expression [60,93]. This points towards itaconate likely playing a similar role to
552 succinate in the macrophage [60], where it acts as an important signalling molecule rather than as a
553 carbon source. This is supported by both the shared transport machinery and catabolite repression
554 mechanisms of the two molecules. Despite this, the importance of an intact itaconate degradation
555 pathway during infection is clear and continues to be shown in studies; suggesting that it is a valid target
556 for the development of novel antibacterials, which was the goal of one previous study [103]. The effects
557 of itaconate under other infection-relevant conditions, such as at low pH—where itaconate has been
558 shown to have more potent antibacterial activity—is an area of study that may also reveal considerably
559 different metabolic effects [17]. This work has expanded on our understanding of STm itaconate
560 degradation and the important interplay with other stress responses. Furthermore, using a media with

561 itaconate as a sole carbon source enables high throughput screening of potential itaconate degradation
562 inhibitors as an alternative treatment against intra-macrophage STm or other itaconate degrading
563 bacteria.

565 Methods

566 ***Chemicals, media and bacteria strains***

567 All chemicals, BD Difco™ Nutrient broth/agar (NB/NA), and Mueller-Hinton broth II (MHB)
568 were purchased from Millipore-Sigma (Canada), Thermo Fisher Scientific (Canada) or Chem-Impex
569 (USA) unless otherwise stated. M9 media was prepared from the following components: M9 salts (48
570 mM Na_2HPO_4, 22 mM KH_2PO_4, 8.6 mM NaCl, 18.7 mM NH_4Cl), 2 mM $MgSO_4$, 0.1 mM $CaCl_2$, trace
571 metals (30 μM $FeCl_3$, 25 μM Na_2EDTA, 8 μM $ZnCl_2$, 3 μM H_3BO_3, 3 μM $MnCl_2$, 2 μM $(NH_4)_6Mo_7O_{24}$,
572 2 μM $CuCl_2$, 2 μM $CoCl_2$), and either 0.4% (w/v) sodium acetate for M9A, or 10 mM itaconic acid for
573 M9I. The media was adjusted to pH 7.2 before filter sterilizing.

574 *Salmonella* Typhimurium ATCC 14028, *Pseudomonas aeruginosa* ATCC 27853, and RAW
575 264.7 (TIB-71) were purchased from Cedarlane (Canada), and STm mutants (Δ*lgl*, Δ*ict,* Δ*ich,* Δ*ccl,*
576 Δ*itaR*) are from the BEI Resources (www.beiresources.org) collection of single gene deletion (SGD)
577 mutants that were originally constructed by Porwollik *et al.* (2014) [104].

578

579 ***General bacterial growth procedures***

580 Bacteria were routinely grown by first streaking from a glycerol stock on nutrient agar plates
581 (with 50 μg/mL kanamycin for the STm mutants) and grown overnight at 37°C. Generally, 3-5 colonies
582 were picked and transferred to 5 mL liquid cultures using the appropriate broth and antibiotic. Cultures
583 were grown overnight at 37°C and 250 rpm. Stationary phase cultures were subcultured at a minimum
584 1/100 dilution into the appropriate fresh media and grown to a mid-exponential phase (OD ≈ 0.3-0.7)
585 before use in experiments. Bacteria grown in minimal media were subcultured additional times (2
586 subcultures minimum in M9A and 3 subcultures minimum in M9I, unless otherwise stated) before use in
587 experiments to allow for the bacteria to sufficiently adapt to the media. ODs were monitored using either

588 a Cary 60 UV-Vis spectrophotometer (Agilent Technologies) or a SpectraMax i3x microplate reader
589 (Molecular Devices). Bacterial growth curves were fit to Gompertz growth models using Graphpad
590 Prism v9.0 (Graphpad Software) and doubling times were extracted using the Dashing Growth
591 Curves[105] web application: https://dashing-growth-curves.ethz.ch/.
592
593 ***Minimum inhibitory concentration (MIC)***
594 MIC assays were performed following the microplate dilution antimicrobial susceptibility testing
595 outlined in the CLSI guidelines with a few modifications [106]. Briefly, itaconic acid was dissolved to 1
596 M in M9A media and the pH was adjusted back to pH 7.2 to ensure no effect from pH changes as
597 previously reported [17]. Serial dilutions were made in 96-well plates at the desired concentrations.
598 Mid-exponential phase M9A-adapted bacteria were added at 5×10^5 CFU/mL and the plates were sealed
599 with a gas permeable moisture barrier seal (FroggaBio, Canada) to prevent excessive evaporation,
600 before incubation at 37°C and 350 rpm, using a tabletop orbital plate shaker (OHAUS, USA). Growth
601 was measured at OD 600 by microplate reader. The plate was monitored until there was visible growth
602 in the untreated control ($OD_{600} > 0.2$, ~36 h). The data was fit to a Gompertz non-linear regression
603 [107], allowing for calculation of the MIC using Graphpad Prism v9.0. All MICs were done in a
604 biological triplicate.
605
606 ***Biofilm assays***
607 Biofilm formation was quantified in 96-well plates using the methods established by Coffey and
608 Anderson (2014) [108]. After either growth or MIC measurement, the suspended bacteria were first
609 removed from the plate, before washing the plate twice with excess H_2O, and staining the plate with
610 200 µL of 0.1% (w/v) crystal violet for 10 min at room temperature (RT). The plates were then rinsed

611 four times with excess H_2O, before allowing them to dry at RT overnight. Once dry, the stained biofilm
612 was solubilized in 200 µL 30% acetic acid, incubated with shaking (350 rpm) for 10 min at RT, and the
613 absorbance was measured at 550 nm. Biofilm formation in MHB, M9A, and M9I was measured at
614 stationary phase (OD_{600} ~0.35, ~0.32, and ~0.19, respectively in 100 µL/well), and the experiment was
615 done in triplicate.
616
617 ***Macrophage infection assay***
618 Raw 264.7 mouse macrophages were cultured in Dulbecco's Modified Eagle Medium (DMEM)
619 with 10% fetal bovine serum (FBS) and grown at 37ºC in a 5% CO_2 atmosphere. A cell scraper was used
620 to lift cells off the flask when passaging (rather than trypsin). Macrophages were seeded in 96-well
621 plates at 1 x 10^4 cells per well (100 µL; measured by haemocytometer) and allowed to adhere for ~16 h
622 before the experiment. On the day of the experiment, STm strains were subcultured 1/100 in NB and
623 allowed to grow to mid-exponential phase. The culture was diluted in NB to an OD = 0.1, diluted 1/10
624 into DMEM + 10% FBS to opsonize the bacteria, and allowed to incubate statically for 1 h at 37ºC and
625 5% CO_2. Bacteria were then further diluted to achieve a multiplicity of infection (MOI) of 10 bacteria
626 cells per macrophage in each well (in 100 µL) for the STm SGD mutant experiment or an MOI of 15 in
627 the M9I-adapted STm strain experiment (see below for extra details). The plates were centrifuged at
628 500 × g for 2 min to sediment the STm cells and increase contact with the macrophages, before
629 incubating at 37ºC and 5% CO_2. This was designated time zero. After 30 min of infection, the media
630 was removed and replaced with fresh DMEM (10% FBS) containing 100 µg/mL gentamicin to kill the
631 extracellular bacteria. The plates were incubated for 30 min at 37ºC in 5% CO_2, before removing and
632 replacing the media once again with DMEM (10% FBS) with 10 µg/mL gentamicin. The cells were
633 incubated as before for ~20 h. To count the amount of intracellular STm, the macrophages were first

634 washed with phosphate-buffered saline (PBS; 2 × 200 μL per well) and then lysed with 0.1% Triton X-
635 100 in PBS, scraping using a pipette tip and forceful pipetting without the formation of bubbles. The
636 lysates were diluted as needed in PBS and plated on NA for CFU counting. To minimize random error,
637 the experiment was performed in two separate and identical plates, the samples of which were combined
638 before plating. Within each plate, 3 biological replicates (from different initial bacterial cultures) were
639 included in technical duplicate, and the experiment was repeated three or four times (n = 18-24).
640 Outliers were tested and removed using the ROUT method on Graphpad Prism and statistical differences
641 were calculated using a one-way ANOVA with multiple comparisons (for the STm SGD mutants) or a
642 two-tailed t-test (for the M9I-adapted mutant). Due to high variability in the MOI across experiments
643 (from the random error associated with diluting bacterial suspensions), in parallel with macrophage
644 infection, the bacteria used for the infection were enumerated by serially diluting in PBS and plating on
645 NA for CFU counting to confirm the true MOI of the sample. Outliers were tested using the ROUT
646 method and infection results were removed from samples with outlier MOIs. A one-way ANOVA or
647 two-tailed t-test were used to ensure no significant difference ($p > 0.989$) between conditions (**S5 Fig**).
648

649 ***Whole Genome Sequencing of M9A- and M9I-adapted STm***

650 Growths started from a single colony on NA, which was allowed to grow to stationary phase in
651 NB prior to being subcultured 1/100 in either M9A or M9I, each in triplicate. A sample of the starting
652 culture in NB was taken and the DNA was extracted using a Bio Basic (Canada) EZ-10 genomic DNA
653 miniprep kit. M9A/M9I-adapted cultures were grown until they reached stationary phase before
654 subculturing. After three subcultures, cells were collected, and their DNA was extracted for sequencing.
655 Whole genome sequencing was performed at SeqCenter (Pittsburgh, PA, USA) using the Illumina
656 NovaSeq X Plus. The sequencing depth was on average 350×. The Breseq v0.37.1 pipeline [109] was

657 used for variant calling with the polymorphism flag. The genomes were deposited on the NCBI
658 database, Submission ID (SUB15249457), BioProject ID (PRJNA1249104). The reference sequence for
659 *Salmonella enterica* serovar Typhimurium ATCC 14028 used for variant calling is available at:
660 genomes.atcc.org/genomes/814482244337467e?tab=overview-tab.
661

662 ***STm growth and extraction for metabolomics***

663 Media-adapted cultures (as described above) were washed once with their respective media
664 before resuspending in 50 mL cultures in 250 mL Erlenmeyer flasks at an OD of 0.001 for MHB, or 0.1
665 for M9A and M9I before allowing to grow at 37ºC, 250 rpm. The OD at stationary phase for each media
666 under these conditions was established as 2.5 for MHB, 1.6 for M9A, and 1.1 for M9I. Samples were
667 taken at two phases of growth: mid-exponential phase (EP) samples were collected when cultures were
668 at 0.3× the stationary OD, and early-stationary phase (SP) samples were collected when cultures were at
669 0.9× the stationary OD for the respective media. Once cultures reach the appropriate ODs, a sample was
670 taken and diluted in the appropriate media to get 13 mL of OD = 0.25, which allowed us to normalize
671 how much biomass was collected across all conditions. The cells were pelleted by centrifugation in a 15
672 mL tube at 14 000 × g and 4ºC for 10 min. All but 1.5 mL of the supernatant was removed, then the cells
673 were resuspended and transferred to a 2 mL microfuge tube to be pelleted again. The cells were washed
674 1× with ice-cold 150 mM ammonium formate, pH 7.4, before centrifugation at 21 000 × g and 4ºC for 5
675 min, before removing the supernatant. The cells were frozen at -80 ºC for 1-2 days before extraction.
676 Additionally, no-cell media controls were made by processing a sample of each media the same as
677 cellular pellets to identify background ion signals present in the media rather than the cell extracts.
678 The samples were always kept on ice during the extraction process. Cell pellets were lysed and
679 extracted by first resuspending them in 380 µL of 50% MeOH/H_2O (v/v), before adding 220 µL of

680 MeCN and 6 ceramic beads (1.4 mm) per sample. Cells were lysed and homogenized by bead-beating
681 for 2 minutes at 30 Hz using a QIAGEN TissueLyser II (Germany). Next, 600 µL of ice-cold DCM and
682 400 µL of ice-cold water were added to each sample, and the mixture was vortexed for 1 min before
683 allowing the metabolites to partition on ice for 10 min. Lastly, the mixtures were centrifuged at 1500 × *g*
684 and 1ºC for 10 min. A 700 µL aliquot of the aqueous layer was collected and dried by vacuum
685 centrifugation (Labconco, USA) at -4°C before being stored at -80 ºC until analysis.
686
687 ***Data collection for targeted metabolomics of short chain CoA metabolites***
688 For analysis of short chain CoA metabolites, samples were injected onto an Agilent 6470 Triple
689 Quadrupole (QQQ)–LC–MS/MS (Agilent Technologies). Chromatographic separation of the
690 metabolites was achieved using a 1290 Infinity ultra-performance quaternary pump liquid
691 chromatography system (Agilent Technologies, USA). The mass spectrometer was equipped with a Jet
692 StreamTM electrospray ionization source, and samples were analyzed in negative mode. The source-gas
693 temperature and flow were set at 300°C and 5 L/min, respectively, the nebulizer pressure was set at
694 45 psi, and the capillary voltage was set at 3,500 V. Multiple reaction monitoring parameters
695 (qualifier/quantifier ions and retention times) were optimized and validated using authentic metabolite
696 standards. Metabolite standards were run at multiple stages along the data acquisition workflow, which
697 were used as quality control (QC) samples in the analysis.
698 Dried extracts were re-suspended in 50 µL of chilled H_2O, clarified by centrifugation at 1°C, and
699 transferred to glass inserts before injection. Sample injection volumes for analyses were 5 µL.
700 Chromatographic separation was achieved using a XBridge C18 column 3.5 µm, 2.1 × 150 mm
701 (Waters). The chromatographic gradient started at 100% mobile phase A (10 mM ammonium acetate in
702 water) with a 15 min gradient to 35% B (MeCN) at a flow rate of 0.2 mL/min. This was followed by an

703 increase to 100% B over 0.1 min, a 4.9 min hold time at 100% mobile phase B and a subsequent re-
704 equilibration time (6 min) at 100% A before the next injection.
705
706 ***Data collection for ion pairing targeted metabolomic of central carbon metabolism***
707 After extracts were sampled for CoA metabolites, they were analyzed using an ion pairing
708 method on the same instrument as described above. The source-gas temperature and flow were set at
709 150°C and 13 L min^{-1}, respectively, the nebulizer pressure was set at 45 psi, and the capillary voltage
710 was set at 2,000 V. As above, QC samples made up of authentic metabolite standards were used to
711 validate parameters.
712 Chromatographic separation of the isomers and other metabolites was achieved by using a
713 Zorbax Extend C18 column 1.8 µm, 2.1 × 150 mm with guard column 1.8 µm, 2.1 × 5 mm (Agilent
714 Technologies). The chromatographic gradient started at 100% mobile phase C (97% water, 3%
715 methanol, 10 mM tributylamine, 15 mM acetic acid, 5 µM medronic acid) at a flow rate of
716 0.25 mL min^{-1} for 2.5 min, followed by a 5-min gradient to 20% mobile phase D (methanol, 10 mM
717 tributylamine, 15 mM acetic acid, 5 µM medronic acid), a 5.5-min gradient to 45% D,a 7-min gradient
718 to 99% D, and finally, a 4-min hold at 100% mobile phase D. The column was restored by washing with
719 99% mobile phase E (90% aqueous MeCN) for 3 min at 0.25 mL min^{-1}, followed by increasing the flow
720 rate to 0.8 mL min^{-1} over 0.5 min and holding for 3.85 min, before returning to 0.6 mL min^{-1} over 0.15
721 min. The column was then re-equilibrated at 100% C over 0.75 min, during which the flow rate was
722 decreased to 0.4 mL min^{-1}, and held for 7.65 min. One minute before the next injection, the flow rate
723 was brought back to 0.25 mL min^{-1}. The column temperature was maintained at 35°C. The metabolite
724 standards used for metabolomics were purchased from Sigma-Aldrich.
725

726 ***Metabolomics Analysis***

727 Peak area data was carefully reviewed to ensure the accuracy and robustness of the analysis. Of
728 the 296 metabolites in the targeted screen panel, ions that had weak or no signal were removed before
729 analysis. The injection blanks and the controls made up of extracts from growth media alone were used
730 to identify and remove metabolite signals that could not be resolved from the background.
731 Metaboanalyst 6.0 [110] was used to perform all metabolomics analyses unless otherwise stated. The
732 data was filtered for reliability and to remove non-informative variables by excluding features that
733 exhibited relative standard deviations (RSDs) greater than 30% of the QC samples, metabolites outside
734 of the 5% interquantile range across all samples, and mean intensities within 5% of the limit of
735 detection. The data was normalized to ensure a Gaussian distribution before analysis by $\log_{10}$
736 transforming and auto scaling the data. Multiple analyses were performed to ensure the robustness of the
737 interpreted results by globally fitting the six experimental conditions in addition to analyzing important
738 paired conditions. In the multiple variable analyses (across all six conditions), significant metabolites
739 were identified by two-way ANOVA ($p < 0.05$). In the pairwise comparisons, T-test ($p < 0.05$) and fold-
740 change ($\log_{10}(FC) > 2$) were used. Volcano plots and heatmaps were made using Graphpad prism and
741 the calculated results or normalized abundances were computed using Metaboanalyst.
742
743
744

746 Supporting Information

747 **S1 Fig**: **Growth data of various STm SPI-13 mutants in M9A and M9I.** This data was summarized in
748 Figure 1b. Error bars depict the SD. n =3.

749 **S2 Fig**: **Gentamicin protection assay comparing the infection of STm wt and Δ*ich* from 1 h to 72 h.**
750 Dotted lines and coloured bands depict the SD around each point connected by a straight line between
751 point. n=4 per timepoint.

752 **S3 Fig: Overlap of genetic mutations within the three replicates of STm adapted to (A) M9A or**
753 **(B) M9I.** Genes with mutations that were found at frequencies below 25% are coloured in red and are
754 not bolded, while those found at frequencies above 25% that may have conferred an advantage for
755 growth in that specific media are in bold.

756 **S4 Fig: Comparing relevant pairs of conditions in the metabolomic experiments.** (A) Volcano plots
757 for pairwise comparisons between M9I vs M9A or MHB and M9A vs MHB at both EP and SP.
758 Highlighted metabolites were considered significant when log10(FC) > 2 and p-value < 0.05. (B) Venn
759 diagram showing the overlap of significant metabolites between the three media (after combing the EP
760 and SP results for each media). Results were stratified to better understand the effects on different
761 pathways by pooling significant features from different comparisons and performing a pathway
762 enrichment analysis. (C) "M9 vs MHB" pooled significant features in the M9A/I vs MHB (EP and SP)
763 comparisons and (D) "M9I vs other" pooled both sets of M9I vs MHB/M9A (EP and SP) comparisons.

764 **S5 Fig**: **MOI of the inoculum used for gentamicin protection assay.** (A) Comparing STm SPI-13
765 mutants to wt STm and (B) comparing STm wt to M9I-adapted STm.

766

767 **S1 Table**: **Background mutations observed prior to the M9A/M9I-adaptation experiments after**
768 **initial growth in MHB.**

769

770 **S1 Appendix. Compilation of all supporting figures and table referenced in the main text of this**

771 **study.** Includes captioned images of S1 Fig, S2 Fig, S3 Fig, S4 Fig, S5 Fig, S1 Table.

772

773 **S1 Data. Raw peak intensity data used for the metabolomics analysis presented in this study.**

774

775 Acknowledgements

776 We would like to thank Prof. Eric Brown at McMaster University for gifting us the *Salmonella*

777 Typhimurium mutant strains. Metabolites were analysed at the Rosalind and Morris Goodman Cancer

778 Institute's Metabolomics Innovation Resource, McGill University. This facility is supported by the

779 Terry Fox Foundation, Quebec Breast Cancer Foundation, The Dr. R. John Fraser and Mrs. Clara M.

780 Fraser Memorial Trust, and McGill University.

781

782 Author Contributions

783 **Conceptualization**: Jacob Pierscianowski, Karine Auclair

784 **Data curation**: Jacob Pierscianowski, Farhan R. Chowdhury

785 **Formal analysis**: Jacob Pierscianowski, Farhan R. Chowdhury

786 **Funding acquisition**: Andréanne Lupien, Brandon L. Findlay, Karine Auclair

787 **Investigation**: Jacob Pierscianowski, Suzana Diaconescu-Grabari, Farhan R. Chowdhury

788 **Methodology**: Jacob Pierscianowski, Farhan R. Chowdhury, Brandon L. Findlay, Karine Auclair

789 **Project administration**: Karine Auclair

790 **Resources**: Jacob Pierscianowski, Suzana Diaconescu-Grabari, Andréanne Lupien, Karine Auclair

791 **Supervision**: Brandon L. Findlay, Karine Auclair

792 **Validation**: Jacob Pierscianowski, Karine Auclair

793 **Visualization**: Jacob Pierscianowski

794 **Writing –original draft**: Jacob Pierscianowski

795 **Writing –review & editing**: Jacob Pierscianowski, Farhan R. Chowdhury, Brandon L. Findlay, Karine

796 Auclair

797

798 Data Availability Statement

799 All relevant data are within the paper and its Supporting Information.

800

801 Funding

802 This research was funded by the Canadian Institute of Health Research (CIHR grant PJT-166175) to

803 K.A. and the FRQ-funded Réseau Québecois de Recherche sur les Médicaments (RQRM grant 78855)

804 to K.A. and B.L.F. NSERC and FRQS are also thanked for scholarships to J.P. (CGSM and PGSD) and

805 F.R.C. (B2X Graduate Studentship), respectively. The funders had no role in study design, data

806 collection and analysis, decision to publish, or preparation of the manuscript.

807

808 Competing Interests

809 The authors declare no competing interests.

810

References

1. Majowicz SE, Musto J, Scallan E, Angulo FJ, Kirk M, O'Brien SJ, et al. The Global Burden of Nontyphoidal Salmonella Gastroenteritis. Clinical Infectious Diseases. 2010;50: 882–889. doi:10.1086/650733

2. Lamichhane B, Mawad AMM, Saleh M, Kelley WG, Harrington PJ, Lovestad CW, et al. Salmonellosis: An Overview of Epidemiology, Pathogenesis, and Innovative Approaches to Mitigate the Antimicrobial Resistant Infections. Antibiotics. 2024;13: 76. doi:10.3390/antibiotics13010076

3. Chlebicz A, Śliżewska K. Campylobacteriosis, Salmonellosis, Yersiniosis, and Listeriosis as Zoonotic Foodborne Diseases: A Review. International Journal of Environmental Research and Public Health. 2018;15: 863. doi:10.3390/ijerph15050863

4. WHO Bacterial Priority Pathogens List 2024: Bacterial Pathogens of Public Health Importance, to Guide Research, Development, and Strategies to Prevent and Control Antimicrobial Resistance. 1st ed. Geneva: World Health Organization; 2024.

5. Kehl A, Noster J, Hensel M. Eat in or Take out? Metabolism of Intracellular Salmonella enterica. Trends in Microbiology. 2020;28: 644–654. doi:10.1016/j.tim.2020.03.005

6. Thompson A, Fulde M, Tedin K. The metabolic pathways utilized by Salmonella Typhimurium during infection of host cells. Environmental Microbiology Reports. 2018;10: 140–154. doi:10.1111/1758-2229.12628

7. Bumann D, Schothorst J. Intracellular Salmonella metabolism. Cellular Microbiology. 2017;19: e12766. doi:10.1111/cmi.12766

8. Raghunathan A, Reed J, Shin S, Palsson B, Daefler S. Constraint-based analysis of metabolic capacity of Salmonella typhimurium during host-pathogen interaction. BMC Syst Biol. 2009;3: 38. doi:10.1186/1752-0509-3-38

9. Bumann D, Cunrath O. Heterogeneity of Salmonella-host interactions in infected host tissues. Current Opinion in Microbiology. 2017;39: 57–63. doi:10.1016/j.mib.2017.09.008

10. Fanous J, Claudi B, Tripathi V, Li J, Goormaghtigh F, Bumann D. Limited impact of Salmonella stress and persisters on antibiotic clearance. Nature. 2025; 1–9. doi:10.1038/s41586-024-08506-6

11. Kamaruzzaman NF, Kendall S, Good L. Targeting the hard to reach: challenges and novel strategies in the treatment of intracellular bacterial infections. British Journal of Pharmacology. 2017;174: 2225–2236. doi:10.1111/bph.13664

12. Claudi B, Spröte P, Chirkova A, Personnic N, Zankl J, Schürmann N, et al. Phenotypic Variation of Salmonella in Host Tissues Delays Eradication by Antimicrobial Chemotherapy. Cell. 2014;158: 722–733. doi:10.1016/j.cell.2014.06.045

13. Steeb B, Claudi B, Burton NA, Tienz P, Schmidt A, Farhan H, et al. Parallel Exploitation of Diverse Host Nutrients Enhances Salmonella Virulence. PLOS Pathogens. 2013;9: e1003301. doi:10.1371/journal.ppat.1003301

850 14. Carfrae LA, Brown ED. Nutrient stress is a target for new antibiotics. Trends in Microbiology.
851 2023;31: 571–585. doi:10.1016/j.tim.2023.01.002

852 15. Michelucci A, Cordes T, Ghelfi J, Pailot A, Reiling N, Goldmann O, et al. Immune-responsive
853 gene 1 protein links metabolism to immunity by catalyzing itaconic acid production. Proceedings
854 of the National Academy of Sciences. 2013;110: 7820–7825. doi:10.1073/pnas.1218599110

855 16. Chen M, Sun H, Boot M, Shao L, Chang S-J, Wang W, et al. Itaconate is an effector of a Rab
856 GTPase cell-autonomous host defense pathway against Salmonella. Science. 2020;369: 450–
857 455. doi:10.1126/science.aaz1333

858 17. Duncan D, Lupien A, Behr MA, Auclair K. Effect of pH on the antimicrobial activity of the
859 macrophage metabolite itaconate. Microbiology. 2021;167. doi:10.1099/mic.0.001050

860 18. Liu Z, Wang C. Dissecting S-itaconation at host–pathogen interactions with chemical proteomics
861 tools. Current Opinion in Microbiology. 2025;83: 102579. doi:10.1016/j.mib.2025.102579

862 19. Lampropoulou V, Sergushichev A, Bambouskova M, Nair S, Vincent EE, Loginicheva E, et al.
863 Itaconate Links Inhibition of Succinate Dehydrogenase with Macrophage Metabolic Remodeling
864 and Regulation of Inflammation. Cell Metabolism. 2016;24: 158–166.
865 doi:10.1016/j.cmet.2016.06.004

866 20. Chen Y-T, Lohia GK, Chen S, Liu Z, Wong Fok Lung T, Wang C, et al. A host-pathogen
867 metabolic synchrony that facilitates disease tolerance. Nat Commun. 2025;16: 3729.
868 doi:10.1038/s41467-025-59134-1

869 21. Kwai BXC, Collins AJ, Middleditch MJ, Sperry J, Bashiri G, Leung IKH. Itaconate is a covalent
870 inhibitor of the Mycobacterium tuberculosis isocitrate lyase. RSC Med Chem. 2021;12: 57–61.
871 doi:10.1039/d0md00301h

872 22. McFadden BA, Purohit S. Itaconate, an isocitrate lyase-directed inhibitor in Pseudomonas
873 indigofera. Journal of Bacteriology. 1977;131: 136–144. doi:10.1128/jb.131.1.136-144.1977

874 23. Zhang Y, Qin W, Liu D, Liu Y, Wang C. Chemoproteomic profiling of itaconations in Salmonella.
875 Chem Sci. 2021;12: 6059–6063. doi:10.1039/D1SC00660F

876 24. Liu Z, Liu D, Wang C. In situ chemoproteomic profiling reveals itaconate inhibits de novo purine
877 biosynthesis in pathogens. Cell Reports. 2024;43: 114737. doi:10.1016/j.celrep.2024.114737

878 25. Priya M, Gupta SK, Koundal A, Kapoor S, Tiwari S, Kidwai S, et al. Itaconate mechanism of
879 action and dissimilation in Mycobacterium tuberculosis. Proceedings of the National Academy of
880 Sciences. 2025;122: e2423114122. doi:10.1073/pnas.2423114122

881 26. Sasikaran J, Ziemski M, Zadora PK, Fleig A, Berg IA. Bacterial itaconate degradation promotes
882 pathogenicity. Nat Chem Biol. 2014;10: 371–377. doi:10.1038/nchembio.1482

883 27. Wang H, Fedorov AA, Fedorov EV, Hunt DM, Rodgers A, Douglas HL, et al. An essential
884 bifunctional enzyme in *Mycobacterium tuberculosis* for itaconate dissimilation and leucine
885 catabolism. Proc Natl Acad Sci USA. 2019;116: 15907–15913. doi:10.1073/pnas.1906606116

886 28. Adler J, Wang S-F, Lardy HA. The Metabolism of Itaconic Acid by Liver Mitochondria. Journal of
887 Biological Chemistry. 1957;229: 865–879. doi:10.1016/S0021-9258(19)63691-4

888 29. Wang S-F, Adler J, Lardy HA. The Pathway of Itaconate Metabolism by Liver Mitochondria.
889 Journal of Biological Chemistry. 1961;236: 26–30. doi:10.1016/S0021-9258(18)64421-7

890 30. Marcero JR, Cox JE, Bergonia HA, Medlock AE, Phillips JD, Dailey HA. The immunometabolite
891 itaconate inhibits heme synthesis and remodels cellular metabolism in erythroid precursors.
892 Blood Advances. 2021;5: 4831–4841. doi:10.1182/bloodadvances.2021004750

893 31. Schürmann M, Wübbeler JH, Grote J, Steinbüchel A. Novel Reaction of Succinyl Coenzyme A
894 (Succinyl-CoA) Synthetase: Activation of 3-Sulfinopropionate to 3-Sulfinopropionyl-CoA in
895 Advenella mimigardefordensis Strain DPN7T during Degradation of 3,3′-Dithiodipropionic Acid.
896 Journal of Bacteriology. 2011;193: 3078–3089. doi:10.1128/jb.00049-11

897 32. Chakraborty S, Chaudhuri D, Balakrishnan A, Chakravortty D. Salmonella methylglyoxal
898 detoxification by STM3117-encoded lactoylglutathione lyase affects virulence in coordination with
899 Salmonella pathogenicity island 2 and phagosomal acidification. Microbiology. 2014;160: 1999–
900 2017. doi:10.1099/mic.0.078998-0

901 33. Chakraborty S, Gogoi M, Chakravortty D. Lactoylglutathione lyase, a critical enzyme in
902 methylglyoxal detoxification, contributes to survival of Salmonella in the nutrient rich
903 environment. Virulence. 2015;6: 50–65. doi:10.4161/21505594.2014.983791

904 34. Karmakar K, Chakraborty S, Kumar JR, Nath U, Nataraja KN, Chakravortty D. Role of lactoyl-
905 glutathione lyase of Salmonella in the colonization of plants under salinity stress. Research in
906 Microbiology. 2023;174: 104045. doi:10.1016/j.resmic.2023.104045

907 35. Hersch SJ, Navarre WW. The Salmonella LysR Family Regulator RipR Activates the SPI-13-
908 Encoded Itaconate Degradation Cluster. Infect Immun. 2020;88: e00303-20.
909 doi:10.1128/IAI.00303-20

910 36. Ki N, Kim J, Jo I, Hyun Y, Ryu S, Ha N-C. Isocitrate binds to the itaconic acid–responsive LysR-
911 type transcriptional regulator RipR in Salmonella pathogenesis. Journal of Biological Chemistry.
912 2022;298: 102562. doi:10.1016/j.jbc.2022.102562

913 37. Espinoza RA, Silva-Valenzuela CA, Amaya FA, Urrutia ÍM, Contreras I, Santiviago CA.
914 Differential roles for pathogenicity islands SPI-13 and SPI-8 in the interaction of Salmonella
915 Enteritidis and Salmonella Typhi with murine and human macrophages. Biological Research.
916 2017;50: 5. doi:10.1186/s40659-017-0109-8

917 38. Shah DH, Lee M, Park J, Lee J, Eo S, Kwon J, et al. Identification of Salmonella gallinarum
918 virulence genes in a chicken infection model using PCR-based signature-tagged mutagenesis.
919 Microbiology. 2005;151: 3957–3968. doi:10.1099/mic.0.28126-0

920 39. Srikumar S, Kröger C, Hébrard M, Colgan A, Owen SV, Sivasankaran SK, et al. RNA-seq Brings
921 New Insights to the Intra-Macrophage Transcriptome of Salmonella Typhimurium. PLOS
922 Pathogens. 2015;11: e1005262. doi:10.1371/journal.ppat.1005262

923 40. Eriksson S, Lucchini S, Thompson A, Rhen M, Hinton JCD. Unravelling the biology of
924 macrophage infection by gene expression profiling of intracellular Salmonella enterica. Molecular
925 Microbiology. 2003;47: 103–118. doi:10.1046/j.1365-2958.2003.03313.x

926 41. Shi L, Adkins JN, Coleman JR, Schepmoes AA, Dohnkova A, Mottaz HM, et al. Proteomic
927 analysis of Salmonella enterica serovar typhimurium isolated from RAW 264.7 macrophages:
928 identification of a novel protein that contributes to the replication of serovar typhimurium inside
929 macrophages. J Biol Chem. 2006;281: 29131–29140. doi:10.1074/jbc.m604640200

930 42. Zhao Y, Jansen R, Gaastra W, Arkesteijn G, Zeijst BAM van der, Putten JPM van. Identification
931 of Genes Affecting Salmonella enterica Serovar Enteritidis Infection of Chicken Macrophages.
932 Infection and Immunity. 2002 [cited 17 Dec 2021]. doi:10.1128/IAI.70.9.5319-5321.2002

933 43. Pujol C, Grabenstein JP, Perry RD, Bliska JB. Replication of Yersinia pestis in interferon γ-
934 activated macrophages requires ripA, a gene encoded in the pigmentation locus. Proceedings of
935 the National Academy of Sciences. 2005;102: 12909–12914. doi:10.1073/pnas.0502849102

936 44. Haneda T, Ishii Y, Danbara H, Okada N. Genome-wide identification of novel genomic islands
937 that contribute to Salmonella virulence in mouse systemic infection. FEMS Microbiology Letters.
938 2009;297: 241–249. doi:10.1111/j.1574-6968.2009.01686.x

939 45. Santiviago CA, Reynolds MM, Porwollik S, Choi S-H, Long F, Andrews-Polymenis HL, et al.
940 Analysis of Pools of Targeted Salmonella Deletion Mutants Identifies Novel Genes Affecting
941 Fitness during Competitive Infection in Mice. PLOS Pathogens. 2009;5: e1000477.
942 doi:10.1371/journal.ppat.1000477

943 46. Silva CA, Blondel CJ, Quezada CP, Porwollik S, Andrews-Polymenis HL, Toro CS, et al.
944 Infection of Mice by Salmonella enterica Serovar Enteritidis Involves Additional Genes That Are
945 Absent in the Genome of Serovar Typhimurium. Infect Immun. 2012;80: 839–849.
946 doi:10.1128/IAI.05497-11

947 47. Silva-Valenzuela CA, Molina-Quiroz RC, Desai P, Valenzuela C, Porwollik S, Zhao M, et al.
948 Analysis of Two Complementary Single-Gene Deletion Mutant Libraries of Salmonella
949 Typhimurium in Intraperitoneal Infection of BALB/c Mice. Frontiers in Microbiology. 2016;6.
950 Available: https://www.frontiersin.org/article/10.3389/fmicb.2015.01455

951 48. Periaswamy B, Maier L, Vishwakarma V, Slack E, Kremer M, Andrews-Polymenis HL, et al. Live
952 Attenuated S. Typhimurium Vaccine with Improved Safety in Immuno-Compromised Mice. PLOS
953 ONE. 2012;7: e45433. doi:10.1371/journal.pone.0045433

954 49. Kröger C, Colgan A, Srikumar S, Händler K, Sivasankaran SK, Hammarlöf DL, et al. An
955 Infection-Relevant Transcriptomic Compendium for Salmonella enterica Serovar Typhimurium.
956 Cell Host & Microbe. 2013;14: 683–695. doi:10.1016/j.chom.2013.11.010

957 50. Hanko EKR, Minton NP, Malys N. A Transcription Factor-Based Biosensor for Detection of
958 Itaconic Acid. ACS Synth Biol. 2018;7: 1436–1446. doi:10.1021/acssynbio.8b00057

959 51. Sun P, Zhang Z, Wang B, Liu C, Chen C, Liu P, et al. A genetically encoded fluorescent
960 biosensor for detecting itaconate with subcellular resolution in living macrophages. Nat Commun.
961 2022;13: 6562. doi:10.1038/s41467-022-34306-5

962 52. Oscar TP. Growth Kinetics of *Salmonella* Isolates in a Laboratory Medium as Affected by Isolate
963 and Holding Temperature†. Journal of Food Protection. 1998;61: 964–968. doi:10.4315/0362-
964 028X-61.8.964

965 53. Karash S, Liyanage R, Qassab A, Lay JO, Kwon YM. A Comprehensive Assessment of the
966 Genetic Determinants in Salmonella Typhimurium for Resistance to Hydrogen Peroxide Using
967 Proteogenomics. Sci Rep. 2017;7: 17073. doi:10.1038/s41598-017-17149-9

968 54. Riquelme SA, Liimatta K, Wong Fok Lung T, Fields B, Ahn D, Chen D, et al. Pseudomonas
969 aeruginosa Utilizes Host-Derived Itaconate to Redirect Its Metabolism to Promote Biofilm
970 Formation. Cell Metabolism. 2020;31: 1091-1106.e6. doi:10.1016/j.cmet.2020.04.017

971 55. Tomlinson KL, Lung TWF, Dach F, Annavajhala MK, Gabryszewski SJ, Groves RA, et al.
972 Staphylococcus aureus induces an itaconate-dominated immunometabolic response that drives
973 biofilm formation. Nat Commun. 2021;12: 1399. doi:10.1038/s41467-021-21718-y

974 56. Bouillet S, Bauer TS, Gottesman S. RpoS and the bacterial general stress response.
975 Microbiology and Molecular Biology Reviews. 2024;88: e00151-22. doi:10.1128/mmbr.00151-22

976 57. Fang FC, Libby SJ, Buchmeier NA, Loewen PC, Switala J, Harwood J, et al. The alternative
977 sigma factor katF (rpoS) regulates Salmonella virulence. Proc Natl Acad Sci USA. 1992;89:
978 11978–11982. doi:10.1073/pnas.89.24.11978

979 58. Dong T, Schellhorn HE. Role of RpoS in Virulence of Pathogens. Infection and Immunity.
980 2010;78: 887–897. doi:10.1128/iai.00882-09

981 59. Janausch IG, Zientz E, Tran QH, Kröger A, Unden G. C4-dicarboxylate carriers and sensors in
982 bacteria. Biochimica et Biophysica Acta (BBA) - Bioenergetics. 2002;1553: 39–56.
983 doi:10.1016/S0005-2728(01)00233-X

984 60. Wenner N, Zhu X, Rowe WPM, Händler K, Hinton JCD. Succinate utilisation by Salmonella is
985 inhibited by multiple regulatory systems. PLOS Genetics. 2024;20: e1011142.
986 doi:10.1371/journal.pgen.1011142

987 61. Quandt EM, Deatherage DE, Ellington AD, Georgiou G, Barrick JE. Recursive genomewide
988 recombination and sequencing reveals a key refinement step in the evolution of a metabolic
989 innovation in Escherichia coli. Proceedings of the National Academy of Sciences. 2014;111:
990 2217–2222. doi:10.1073/pnas.1314561111

991 62. Amin MR, Korchinski L, Yoneda JK, Thakkar R, Sanson CLA, Fitzgerald SF, et al. A mutation in
992 the putative CRP binding site of the dctA promoter of Salmonella enterica serovar Typhimurium
993 enables growth with low orotate concentrations. Can J Microbiol. 2022;68: 615–621.
994 doi:10.1139/cjm-2022-0120

995 63. Nickerson CA, Curtiss R. Role of sigma factor RpoS in initial stages of Salmonella typhimurium
996 infection. Infect Immun. 1997;65: 1814–1823.

997 64. de la Peña Mattozzi M, Kang Y, Keasling JD. Feast: Choking on Acetyl-CoA, the Glyoxylate
998 Shunt, and Acetyl-CoA-Driven Metabolism. In: Timmis KN, editor. Handbook of Hydrocarbon and
999 Lipid Microbiology. Berlin, Heidelberg: Springer; 2010. pp. 1649–1660. doi:10.1007/978-3-540-
1000 77587-4_116

1001 65. Tchawa Yimga M, Leatham MP, Allen JH, Laux DC, Conway T, Cohen PS. Role of
1002 Gluconeogenesis and the Tricarboxylic Acid Cycle in the Virulence of Salmonella enterica
1003 Serovar Typhimurium in BALB/c Mice. Infection and Immunity. 2006;74: 1130–1140.
1004 doi:10.1128/iai.74.2.1130-1140.2006

1005 66. Clark DP, Cronan JE. Two-Carbon Compounds and Fatty Acids as Carbon Sources. EcoSal
1006 Plus. 2005;1: 10.1128/ecosalplus.3.4.4. doi:10.1128/ecosalplus.3.4.4

1007 67. Sarkhel R, Apoorva S, Priyadarsini S, Sridhar HB, Bhure SK, Mahawar M. Malate synthase
1008 contributes to the survival of Salmonella Typhimurium against nutrient and oxidative stress
1009 conditions. Sci Rep. 2022;12: 15979. doi:10.1038/s41598-022-20245-0

1010 68. O'Neill LAJ, Artyomov MN. Itaconate: the poster child of metabolic reprogramming in
1011 macrophage function. Nat Rev Immunol. 2019;19: 273–281. doi:10.1038/s41577-019-0128-5

1012 69. Bambouskova M, Gorvel L, Lampropoulou V, Sergushichev A, Loginicheva E, Johnson K, et al.
1013 Electrophilic properties of itaconate and derivatives regulate the IκBζ–ATF3 inflammatory axis.
1014 Nature. 2018;556: 501–504. doi:10.1038/s41586-018-0052-z

1015 70. Deutscher J, Francke C, Postma PW. How Phosphotransferase System-Related Protein
1016 Phosphorylation Regulates Carbohydrate Metabolism in Bacteria. Microbiology and Molecular
1017 Biology Reviews. 2006 [cited 30 Apr 2025]. doi:10.1128/mmbr.00024-06

1018 71. De Witt J, Ernst P, Gätgens J, Noack S, Hiller D, Wynands B, et al. Characterization and
1019 engineering of branched short-chain dicarboxylate metabolism in Pseudomonas reveals
1020 resistance to fungal 2-hydroxyparaconate. Metabolic Engineering. 2023;75: 205–216.
1021 doi:10.1016/j.ymben.2022.12.008

1022 72. Huang Q, Duan C, Ma H, Nong C, Zheng Q, Zhou J, et al. Structural and functional
1023 characterization of itaconyl-CoA hydratase and citramalyl-CoA lyase involved in itaconate
1024 metabolism of *Pseudomonas aeruginosa*. Structure. 2024 [cited 30 Apr 2024].
1025 doi:10.1016/j.str.2024.04.004

1026 73. Mehboob J, Herman R, Elston RC, Afolabi H, Kinniment-Williams E, Woude M van der, et al.
1027 Itaconate utilisation by the human pathogen Pseudomonas aeruginosa requires uptake via the
1028 IctPQM TRAP transporter. bioRxiv; 2025. p. 2025.04.01.646390. doi:10.1101/2025.04.01.646390

1029 74. King T, Ishihama A, Kori A, Ferenci T. A Regulatory Trade-Off as a Source of Strain Variation in
1030 the Species Escherichia coli. Journal of Bacteriology. 2004;186: 5614–5620.
1031 doi:10.1128/jb.186.17.5614-5620.2004

1032 75. Ferenci T. What is driving the acquisition of mutS and rpoS polymorphisms in Escherichia coli?
1033 Trends in Microbiology. 2003;11: 457–461. doi:10.1016/j.tim.2003.08.003

1034 76. Simm R, Ahmad ,Irfan, Rhen ,Mikael, Le Guyon ,Soazig, and Römling U. Regulation of Biofilm
1035 Formation in Salmonella Enterica Serovar Typhimurium. Future Microbiology. 2014;9: 1261–
1036 1282. doi:10.2217/fmb.14.88

1037 77. Robbe-Saule V, Lopes MD, Kolb A, Norel F. Physiological Effects of Crl in Salmonella Are
1038 Modulated by σS Level and Promoter Specificity. Journal of Bacteriology. 2007;189: 2976–2987.
1039 doi:10.1128/jb.01919-06

1040 78. Steenackers H, Hermans K, Vanderleyden J, De Keersmaecker SCJ. *Salmonella* biofilms: An
1041 overview on occurrence, structure, regulation and eradication. Food Research International.
1042 2012;45: 502–531. doi:10.1016/j.foodres.2011.01.038

1043 79. White AP, Weljie AM, Apel D, Zhang P, Shaykhutdinov R, Vogel HJ, et al. A Global Metabolic
1044 Shift Is Linked to Salmonella Multicellular Development. PLOS ONE. 2010;5: e11814.
1045 doi:10.1371/journal.pone.0011814

1046 80. Ranieri MR, Whitchurch CB, Burrows LL. Mechanisms of biofilm stimulation by subinhibitory
1047 concentrations of antimicrobials. Current Opinion in Microbiology. 2018;45: 164–169.
1048 doi:10.1016/j.mib.2018.07.006

1049 81. Yaeger LN, French S, Brown ED, Côté JP, Burrows LL. Central metabolism is a key player in E .
1050 coli biofilm stimulation by sub-MIC antibiotics. PLoS Genetics. 2023;19: e1011013.
1051 doi:10.1371/journal.pgen.1011013

1052 82. Xie LY, Xu YB, Ding XQ, Liang S, Li DL, Fu AK, et al. Itaconic acid and dimethyl itaconate exert
1053 antibacterial activity in carbon-enriched environments through the TCA cycle. Biomedicine &
1054 Pharmacotherapy. 2023;167: 115487. doi:10.1016/j.biopha.2023.115487

1055 83. Schubert C, Unden G. C4-Dicarboxylates as Growth Substrates and Signaling Molecules for
1056 Commensal and Pathogenic Enteric Bacteria in Mammalian Intestine. Journal of Bacteriology.
1057 2022;204: e00545-21. doi:10.1128/jb.00545-21

1058 84. Unden G, Strecker A, Kleefeld A, Kim OB. C4-Dicarboxylate Utilization in Aerobic and Anaerobic
1059 Growth. EcoSal Plus. 2016;7: 10.1128/ecosalplus.ESP-0021–2015. doi:10.1128/ecosalplus.esp-
1060 0021-2015

1061 85. Spiga L, Winter MG, de Carvalho TF, Zhu W, Hughes ER, Gillis CC, et al. An oxidative central
1062 metabolism enables Salmonella to utilize microbiota-derived succinate. Cell Host Microbe.
1063 2017;22: 291-301.e6. doi:10.1016/j.chom.2017.07.018

1064 86. Jiang L, Wang P, Song X, Zhang H, Ma S, Wang J, et al. Salmonella Typhimurium reprograms
1065 macrophage metabolism via T3SS effector SopE2 to promote intracellular replication and
1066 virulence. Nat Commun. 2021;12: 879. doi:10.1038/s41467-021-21186-4

1067 87. Bowden SD, Rowley G, Hinton JCD, Thompson A. Glucose and Glycolysis Are Required for the
1068 Successful Infection of Macrophages and Mice by Salmonella enterica Serovar Typhimurium.
1069 Infection and Immunity. 2009;77: 3117–3126. doi:10.1128/IAI.00093-09

1070 88. Bowden SD, Ramachandran VK, Knudsen GM, Hinton JCD, Thompson A. An Incomplete TCA
1071 Cycle Increases Survival of Salmonella Typhimurium during Infection of Resting and Activated
1072 Murine Macrophages. May RC, editor. PLoS ONE. 2010;5: e13871.
1073 doi:10.1371/journal.pone.0013871

1074 89. Mitosch K, Beyß M, Phapale P, Drotleff B, Nöh K, Alexandrov T, et al. A pathogen-specific
1075 isotope tracing approach reveals metabolic activities and fluxes of intracellular Salmonella. PLOS
1076 Biology. 2023;21: e3002198. doi:10.1371/journal.pbio.3002198

1077 90. Rosenberg G, Yehezkel D, Hoffman D, Mattioli CC, Fremder M, Ben-Arosh H, et al. Host
1078 succinate is an activation signal for Salmonella virulence during intracellular infection. Science.
1079 2021;371: 400–405. doi:10.1126/science.aba8026

1080 91. Schubert C, Unden G. Regulation of Aerobic Succinate Transporter dctA of E. coli by cAMP-
1081 CRP, DcuS-DcuR, and EIIAGlc: Succinate as a Carbon Substrate and Signaling Molecule.
1082 Microbial Physiology. 2024;34: 108–120. doi:10.1159/000538095

1083 92. Lee SH, Cirino PC, Gonzalez R. Metabolic engineering of *Escherichia coli* for the utilization of
1084 methylsuccinate, the product of methane activation via fumarate addition. Bioresource
1085 Technology. 2024; 131700. doi:10.1016/j.biortech.2024.131700

1086 93. Hersch SJ, Radan B, Ilyas B, Lavoie P, Navarre WW. A stress-induced block in dicarboxylate
1087 uptake and utilization in Salmonella. J Bacteriol. 2021; JB.00487-20. doi:10.1128/JB.00487-20

1088 94. Lévi-Meyrueis C, Monteil V, Sismeiro O, Dillies M-A, Monot M, Jagla B, et al. Expanding the
1089 RpoS/σS-Network by RNA Sequencing and Identification of σS-Controlled Small RNAs in
1090 Salmonella. PLOS ONE. 2014;9: e96918. doi:10.1371/journal.pone.0096918

1091 95. Lévi-Meyrueis C, Monteil V, Sismeiro O, Dillies M-A, Kolb A, Monot M, et al. Repressor activity of
1092 the RpoS/σS-dependent RNA polymerase requires DNA binding. Nucleic Acids Research.
1093 2015;43: 1456–1468. doi:10.1093/nar/gku1379

1094 96. Kröger C, Dillon SC, Cameron ADS, Papenfort K, Sivasankaran SK, Hokamp K, et al. The
1095 transcriptional landscape and small RNAs of Salmonella enterica serovar Typhimurium.
1096 Proceedings of the National Academy of Sciences. 2012;109: E1277–E1286.
1097 doi:10.1073/pnas.1201061109

1098 97. Zheng L, Cardaci S, Jerby L, MacKenzie ED, Sciacovelli M, Johnson TI, et al. Fumarate induces
1099 redox-dependent senescence by modifying glutathione metabolism. Nat Commun. 2015;6: 6001.
1100 doi:10.1038/ncomms7001

1101 98. Sullivan LB, Martinez-Garcia E, Nguyen H, Mullen AR, Dufour E, Sudarshan S, et al. The Proto-
1102 oncometabolite Fumarate Binds Glutathione to Amplify ROS-Dependent Signaling. Molecular
1103 Cell. 2013;51: 236–248. doi:10.1016/j.molcel.2013.05.003

1104 99. Kant S, Liu L, Vazquez-Torres A. The methylglyoxal pathway is a sink for glutathione in
1105 Salmonella experiencing oxidative stress. Baumler AJ, editor. PLoS Pathog. 2023;19: e1011441.
1106 doi:10.1371/journal.ppat.1011441

1107 100. Nguyen TV, Alfaro AC, Young T, Green S, Zarate E, Merien F. Itaconic acid inhibits growth of a
1108 pathogenic marine Vibrio strain: A metabolomics approach. Sci Rep. 2019;9: 5937.
1109 doi:10.1038/s41598-019-42315-6

1110 101. Zhao R, Lei X, Chen J, Yang Y, Guo X, Dai M, et al. Itaconate induces tolerance of
1111 Staphylococcus aureus to aminoglycoside antibiotics. Front Microbiol. 2024;15.
1112 doi:10.3389/fmicb.2024.1450085

1113 102. Loi VV, Busche T, Kuropka B, Müller S, Methling K, Lalk M, et al. Staphylococcus aureus adapts
1114 to the immunometabolite itaconic acid by inducing acid and oxidative stress responses including

1115 S-bacillithiolations and S-itaconations. Free Radical Biology and Medicine. 2023;208: 859–876.
1116 doi:10.1016/j.freeradbiomed.2023.09.031

1117 103. Hammerer F, Chang JH, Duncan D, Ruiz AC, Auclair K. Small Molecule Restores Itaconate
1118 Sensitivity in Salmonella enterica: A Potential New Approach to Treating Bacterial Infections.
1119 ChemBioChem. 2016. doi:10.1002/cbic.201600078

1120 104. Porwollik S, Santiviago CA, Cheng P, Long F, Desai P, Fredlund J, et al. Defined Single-Gene
1121 and Multi-Gene Deletion Mutant Collections in Salmonella enterica sv Typhimurium. PLOS ONE.
1122 2014;9: e99820. doi:10.1371/journal.pone.0099820

1123 105. Reiter MA, Vorholt JA. Dashing Growth Curves: a web application for rapid and interactive
1124 analysis of microbial growth curves. BMC Bioinformatics. 2024;25: 67. doi:10.1186/s12859-024-
1125 05692-y

1126 106. CLSI. Methods for dilution antimicrobial susceptibility tests for bacteria that grow aerobically. 11.
1127 ed. CLSI standard M07. Wayne, PA: Clinical and Laboratory Standards Institute; 2018.

1128 107. Lambert R j. w., Pearson J. Susceptibility testing: accurate and reproducible minimum inhibitory
1129 concentration (MIC) and non-inhibitory concentration (NIC) values. Journal of Applied
1130 Microbiology. 2000;88: 784–790. doi:10.1046/j.1365-2672.2000.01017.x

1131 108. Coffey BM, Anderson GG. Biofilm Formation in the 96-Well Microtiter Plate. In: Filloux A, Ramos
1132 J-L, editors. Pseudomonas Methods and Protocols. New York, NY: Springer; 2014. pp. 631–641.
1133 doi:10.1007/978-1-4939-0473-0_48

1134 109. Deatherage DE, Barrick JE. Identification of Mutations in Laboratory-Evolved Microbes from
1135 Next-Generation Sequencing Data Using breseq. In: Sun L, Shou W, editors. Engineering and
1136 Analyzing Multicellular Systems: Methods and Protocols. New York, NY: Springer; 2014. pp.
1137 165–188. doi:10.1007/978-1-4939-0554-6_12

1138 110. Pang Z, Lu Y, Zhou G, Hui F, Xu L, Viau C, et al. MetaboAnalyst 6.0: towards a unified platform
1139 for metabolomics data processing, analysis and interpretation. Nucleic Acids Research. 2024;52:
1140 W398–W406. doi:10.1093/nar/gkae253

1141

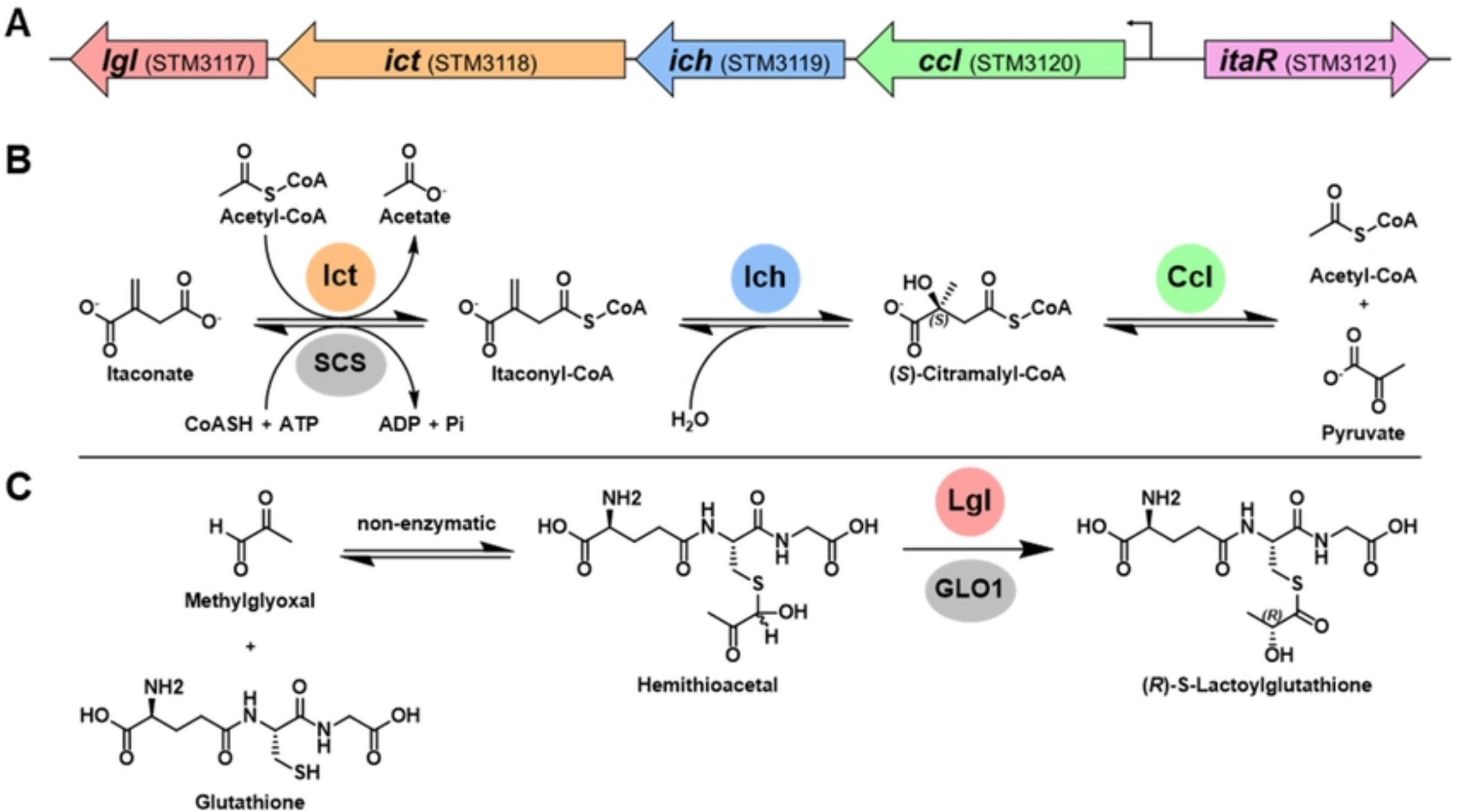
A
lgl (STM3117)
ict (STM3118)
ich (STM3119)
ccl (STM3120)
itaR (STM3121)
B
Acetyl-CoA
Acetate
Ict
SCS
Itaconate
CoASH + ATP
ADP + Pi
Itaconyl-CoA
Ich
H2O
(S)-Citramalyl-CoA
Ccl
Acetyl-CoA
+
Pyruvate
C
Methylglyoxal
+
Glutathione
non-enzymatic
Hemithioacetal
Lgl
GLO1
(R)-S-Lactoylglutathione

Figure 1

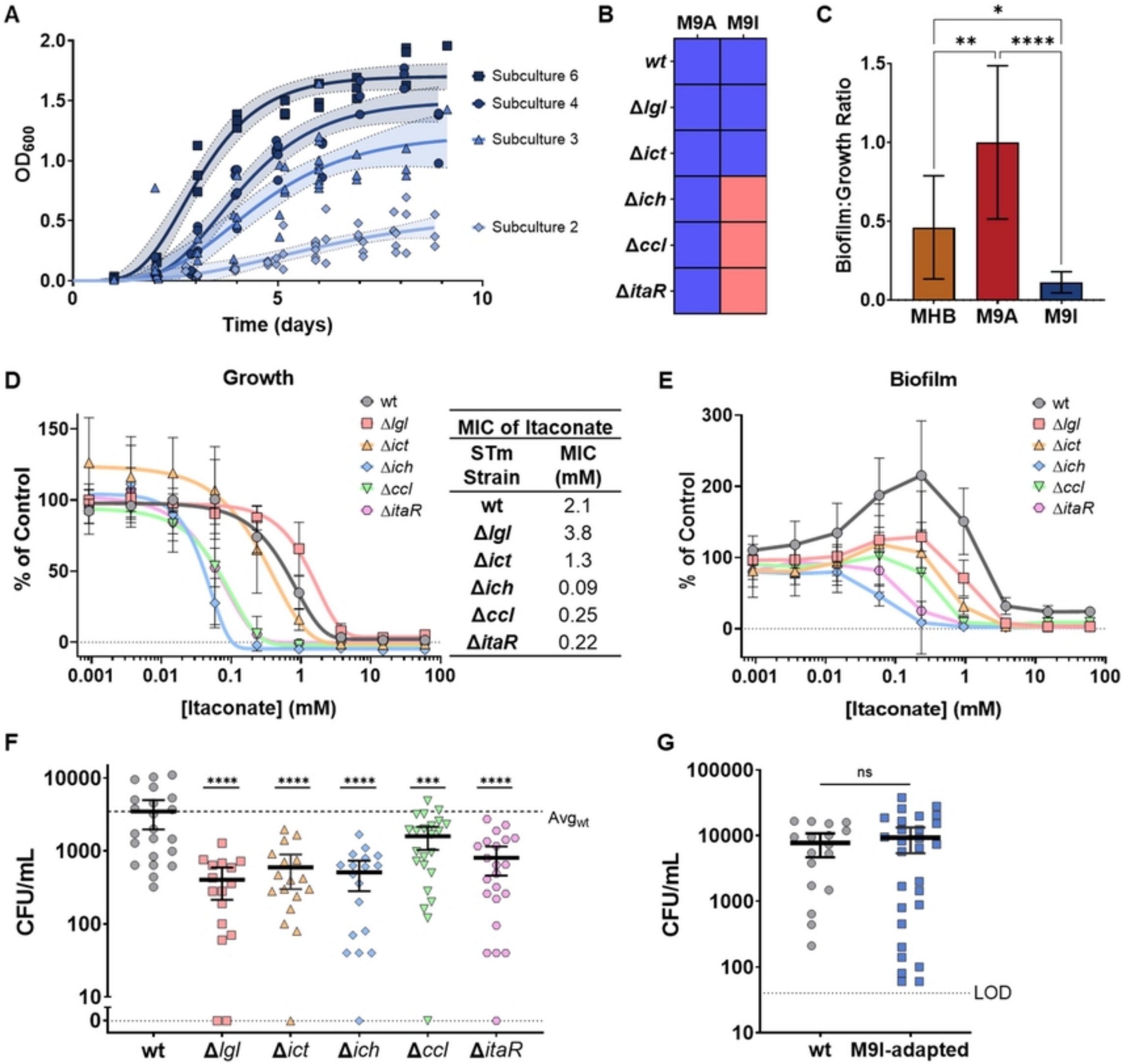
A
OD600
Time (days)
Subculture 6
Subculture 4
Subculture 3
Subculture 2
B
M9A
M9I
wt
Δlgl
Δict
Δich
Δccl
ΔitaR
C
Biofilm:Growth Ratio
MHB
M9A
M9I
D
Growth
% of Control
[Itaconate] (mM)
wt
Δlgl
Δict
Δich
Δccl
ΔitaR
MIC of Itaconate
STm Strain
MIC (mM)
wt 2.1
Δlgl 3.8
Δict 1.3
Δich 0.09
Δccl 0.25
ΔitaR 0.22
E
Biofilm
% of Control
[Itaconate] (mM)
F
CFU/mL
Avgwt
wt
Δlgl
Δict
Δich
Δccl
ΔitaR
G
CFU/mL
ns
LOD
wt
M9I-adapted

Figure 2

stop
ACGGTATCTGTCGCACGAAAATCCTGATTACAAAAGTTAA AAAAGGTCGCGCTTGTGCGAG
pdeK →
DcuR binding site
CRP site 1
CCAGCTCAAACTTTTTAACATTTTTGTTTCAATTATGATCCTGGCGCATTTCTGTCATGTTGT
CRP site 2
-35 box
A or T
C→T G→T
GTGGGTGT + TATTTTAAGGCCGCAGGTTACTCATAACCTTACAAGACCTGTGGTTTTTACTTC
insertion
-10 box
TSS
IscR binding site
SNP
SNP
start
AAGGACACCCT ATGAAAACCTCTCTGTTCAAAAGTCTTTATTTTCAGGTCCTGACAGCAATC
S.D. seq.
dctA →

Figure 3

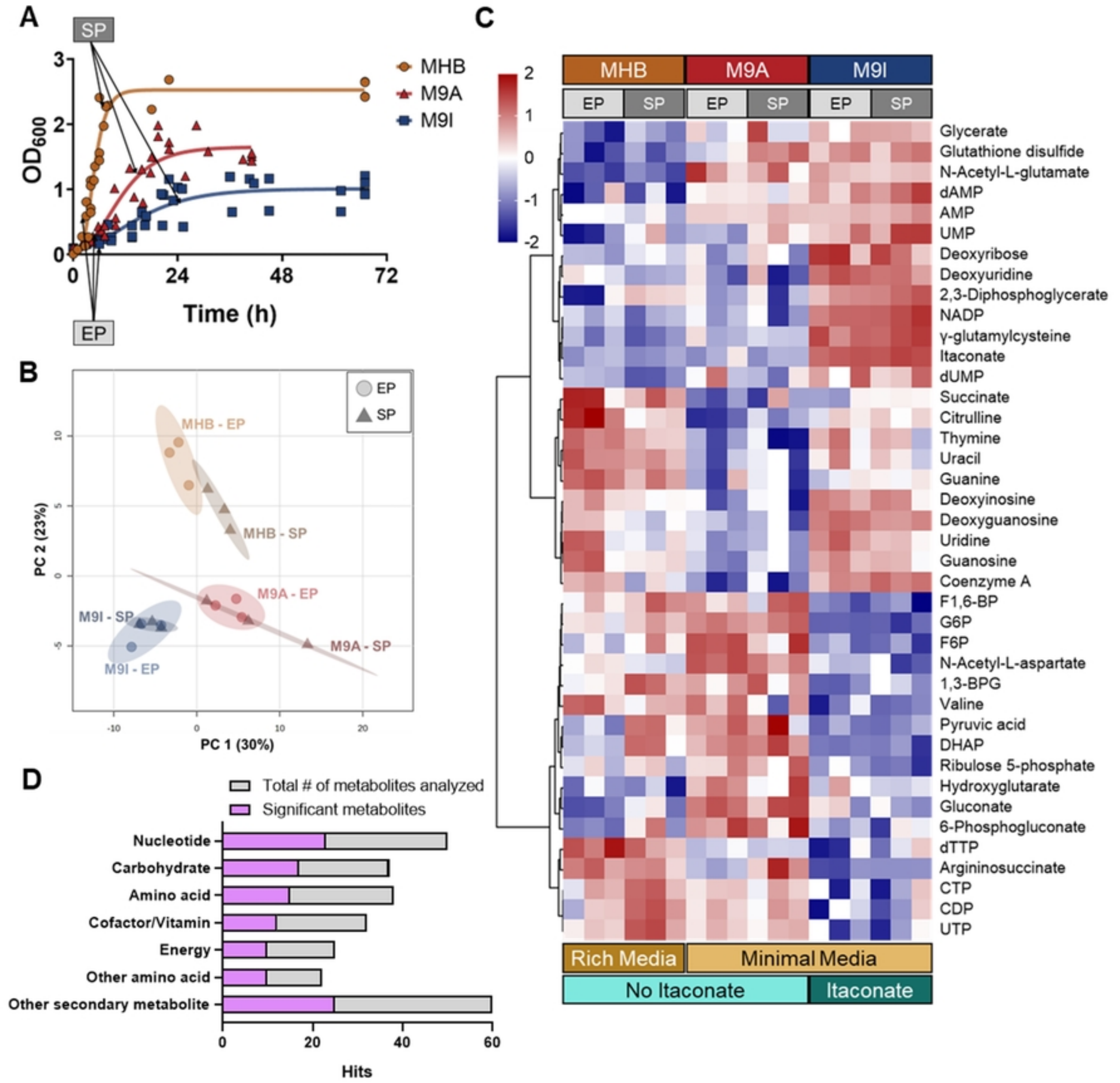
A
SP
EP
MHB
M9A
M9I
OD600
Time (h)
B
EP
SP
MHB - EP
MHB - SP
M9A - EP
M9A - SP
M9I - SP
M9I - EP
PC 2 (23%)
PC 1 (30%)
C
MHB
M9A
M9I
EP
SP
Glycerate
Glutathione disulfide
N-Acetyl-L-glutamate
dAMP
AMP
UMP
Deoxyribose
Deoxyuridine
2,3-Diphosphoglycerate
NADP
γ-glutamylcysteine
Itaconate
dUMP
Succinate
Citrulline
Thymine
Uracil
Guanine
Deoxyinosine
Deoxyguanosine
Uridine
Guanosine
Coenzyme A
F1,6-BP
G6P
F6P
N-Acetyl-L-aspartate
1,3-BPG
Valine
Pyruvic acid
DHAP
Ribulose 5-phosphate
Hydroxyglutarate
Gluconate
6-Phosphogluconate
dTTP
Argininosuccinate
CTP
CDP
UTP
Rich Media
Minimal Media
No Itaconate
Itaconate
D
Total # of metabolites analyzed
Significant metabolites
Nucleotide
Carbohydrate
Amino acid
Cofactor/Vitamin
Energy
Other amino acid
Other secondary metabolite
Hits

Figure 4

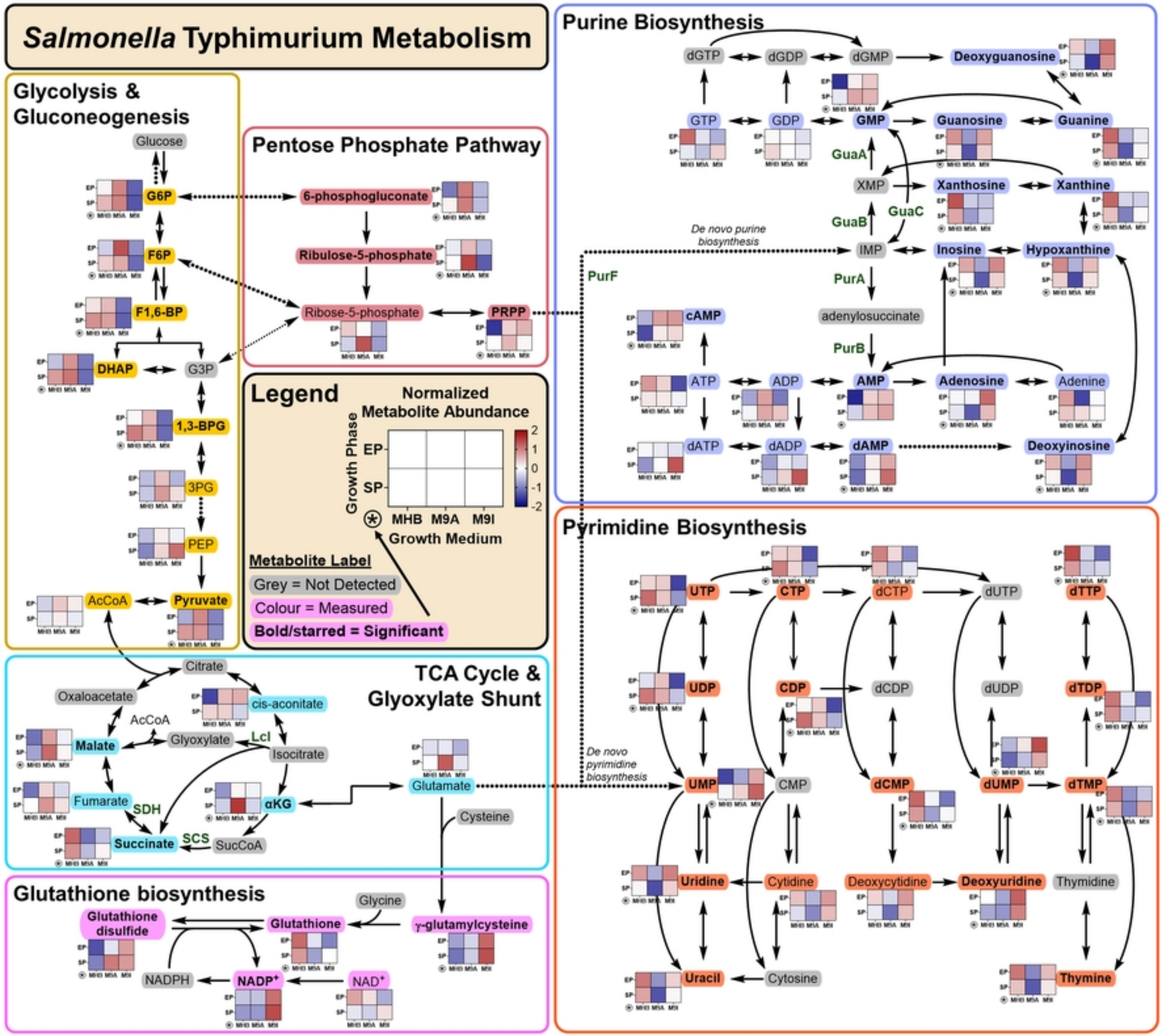
Salmonella Typhimurium Metabolism
Glycolysis & Gluconeogenesis
Glucose
G6P
F6P
F1,6-BP
DHAP
G3P
1,3-BPG
3PG
PEP
AcCoA
Pyruvate
Pentose Phosphate Pathway
6-phosphogluconate
Ribulose-5-phosphate
Ribose-5-phosphate
PRPP
Legend
Normalized Metabolite Abundance
Growth Phase
EP
SP
MHB
M9A
M9I
Growth Medium
Metabolite Label
Grey = Not Detected
Colour = Measured
Bold/starred = Significant
Purine Biosynthesis
dGTP
dGDP
dGMP
Deoxyguanosine
GTP
GDP
GMP
Guanosine
Guanine
GuaA
XMP
Xanthosine
Xanthine
GuaB
GuaC
De novo purine biosynthesis
IMP
Inosine
Hypoxanthine
PurF
PurA
adenylosuccinate
PurB
cAMP
ATP
ADP
AMP
Adenosine
Adenine
dATP
dADP
dAMP
Deoxyinosine
Pyrimidine Biosynthesis
UTP
CTP
dCTP
dUTP
dTTP
UDP
CDP
dCDP
dUDP
dTDP
De novo pyrimidine biosynthesis
UMP
CMP
dCMP
dUMP
dTMP
Uridine
Cytidine
Deoxycytidine
Deoxyuridine
Thymidine
Uracil
Cytosine
Thymine
TCA Cycle & Glyoxylate Shunt
Citrate
Oxaloacetate
cis-aconitate
AcCoA
Malate
Glyoxylate
Lcl
Isocitrate
Fumarate
SDH
αKG
Succinate
SCS
SucCoA
Glutamate
Cysteine
Glutathione biosynthesis
Glycine
Glutathione disulfide
Glutathione
γ-glutamylcysteine
NADPH
NADP+
NAD+

Figure 5